MOUNTAIN-PLAINS CONSORTIUM

MPC 20-419 | D.D. Woolridge, J.D. Niemann, M.A. Perry, K.E. Bauer, and W.T. McCormick III

Quantifying Mountain Basin Runoff Mechanisms for Better Hydrologic Design

Technical Report Documentation Page

1. Report No. MPC-537	2. Government Accession No.	3. Recipient's Catalog No.
4. Title and Subtitle Quantifying Mountain Basin Runoff Mechanisms for Better Hydrologic Design		5. Report Date September 2020
		6. Performing Organization Code
7. Author(s) D.D. Woolridge J.D. Niemann M.A. Perry K.E. Bauer W.T. McCormick III		8. Performing Organization Report No. MPC 20-419
9. Performing Organization Name and Address Colorado State University Campus Delivery 1372 Fort Collins, CO 80523		10. Work Unit No. (TRAIS)
		11. Contract or Grant No.
12. Sponsoring Agency Name and Address Mountain-Plains Consortium North Dakota State University PO Box 6050, Fargo, ND 58108		13. Type of Report and Period Covered Final Report
		14. Sponsoring Agency Code

16. Abstract

Hydrologic analyses are used for dam safety evaluations to determine the flow a dam must pass without failing. They are also used to evaluate bridge and culvert designs from a hydrologic perspective. Many current guidelines model flood runoff solely by an infiltration-excess mechanism. Saturation-excess runoff and subsurface stormflow mechanisms are known to be important for common events in forested regions, but few studies have analyzed their role for extreme events. The objectives of this study are to determine the active streamflow mechanisms for large historical storms and design storms in the Colorado Front Range and to propose methods to model these mechanisms that can be used by consultants. Hydrologic models were developed for five basins to simulate historical events in 1976, 1997, and 2013. The model results show saturation-excess was the dominant mechanism during the 2013 storm, which had a long duration and low rainfall intensities. Infiltration-excess runoff was dominant for the 1976 storm, which had a short duration and high intensities. Surface runoff was not observed during the 1997 storm. Similarly, infiltration-excess dominates for short duration design storms, and saturation-excess dominates for longer design storms.

.

17. Key Word bridge design, culverts, ground transportation, guidelines, hydrology, infrastructure, rainfall, runoff	18. Distribution Statement Public distribution		
19. Security Classif. (of this report) Unclassified	20. Security Classif. (of this page) Unclassified	21. No. of Pages 78	22. Price n/a

Form DOT F 1700.7 (8-72)   Reproduction of completed page authorized

Quantifying Mountain Basin Runoff Mechanisms
for Better Hydrologic Design

Douglas D. Woolridge
Jeffrey D. Niemann (PI)
Mark A. Perry
Kallie E. Bauer
William T. McCormick III

Department of Civil and Environmental Engineering
Colorado State University
Fort Collins, CO 80523

Acknowledgments

Disclaimer

ABSTRACT

Hydrologic analyses are used for dam safety evaluations to determine the flow a dam must pass without failing. They are also used to evaluate bridge and culvert designs. Many current guidelines model flood runoff solely by an infiltration-excess mechanism. Saturation-excess runoff and subsurface stormflow mechanisms are known to be important for common events in forested regions, but few studies have analyzed their role for extreme events. The objectives of this study are to determine the active streamflow mechanisms for large historical storms and design storms in the Colorado Front Range and to propose methods to model these mechanisms that can be used by consultants. Hydrologic models were developed for five basins to simulate historical events in 1976, 1997, and 2013. The model results show saturation-excess was the dominant mechanism during the 2013 storm, which had a long duration and low rainfall intensities. Infiltration-excess runoff was dominant for the 1976 storm, which had a short duration and high intensities. Surface runoff was not observed during the 1997 storm. Similarly, infiltration-excess dominates for short duration design storms, and saturation-excess dominates for longer design storms.

TABLE OF CONTENTS

LIST OF TABLES

LIST OF FIGURES

1. INTRODUCTION

Hydrologic analysis is an important element of dam safety assessments because it determines the design flow a dam must safely pass without overtopping or failing. Hydrologic analysis is also an important component in assessing bridge and culvert designs. Design flows are typically determined by first estimating the rainfall for the probable maximum precipitation (PMP) or a frequency-based design storm. The rainfall is then converted into runoff and ultimately streamflow using hydrologic modeling guidelines. Understanding the active streamflow production mechanisms is a crucial step in determining the basin's outflow hydrograph in response to a given rainfall event. If incorrect mechanisms are assumed, the modeling structure can inadequately simulate the processes occurring in a watershed and inaccurately predict the response to unobserved events (Kirchner 2006; McDonnell et al. 2007).

Many existing guidelines assume runoff is produced by an infiltration-excess mechanism. By this mechanism, runoff occurs when the rainfall intensity exceeds a non-zero infiltration capacity of the soil (Horton 1940). Infiltration-excess runoff is known to be important in arid regions, urban areas, and for soils that have been compacted by humans or animals (Brater 1968; Dunne 1978; Macdonald and Stednick 2003). The Federal Energy Regulatory Commission (FERC) recommends using either the initial and uniform loss method or the Soil Conservation Service (SCS) method in its dam safety guidelines (FERC 2001). When the initial and uniform loss method is used, runoff only occurs when the rainfall intensity exceeds a specified constant infiltration capacity (after the initial loss is met). The United States Bureau of Reclamation guidelines also assume that runoff occurs when the rainfall intensity exceeds a constant infiltration capacity (Cudworth 1989). The State of Colorado typically recommends using the Green and Ampt equation in its dam safety guidelines, which produces runoff when the rainfall intensity exceeds a temporally varying infiltration capacity function (Sabol 2008). However, Perry et al. (2017) found that the Colorado dam safety guidelines overestimate the September 2013 flood in the South Boulder Creek (SBC) basin by more than 300%. Thus, the current guidelines may not reflect realistic hydrologic behavior for the Colorado Front Range.

Streamflow can also be produced by subsurface stormflow and saturation-excess runoff when a low-permeability layer exists at a shallow depth in the soil. Subsurface stormflow occurs when infiltrated water collects on the low-permeability layer and flows downslope to the stream (Kirkby and Chorley 1967). Saturation-excess runoff occurs when rain falls on a location that is completely saturated from the low-permeability layer up to the ground surface (Dunne and Black 1970a). Saturation-excess runoff occurs more frequently at the bottom of hillslopes because the larger upslope area produces more water to saturate the soil and on shallow slopes because they tend to drain to the stream more slowly (Dunne and Black 1970a; Ogden and Watts 2000). While infiltration-excess runoff occurs only if the rainfall intensity exceeds the infiltration capacity, saturation-excess runoff can occur for any intensity if the soil column has completely saturated.

Subsurface stormflow and saturation-excess runoff are known to dominate streamflow production for common events in forested regions. Through an isotope hydrograph separation analysis for a forested region, Pearce et al. (1986) found that a hillslope's streamflow response to small storms was composed primarily of pre-event water that was pushed through the hillslope by newly infiltrated water. The only new water in the streamflow was from direct rainfall on the channel. This result and other similar studies (Hrachowitz et al. 2011; Shanley et al. 2015) suggest the importance of subsurface stormflow to the streamflow hydrograph. In an overview of studies investigating infiltration mechanisms, Dunne (1978) noted that rainfall intensities generally do not exceed soil infiltration capacities for most runoff-producing events in humid regions.

The active streamflow production mechanism in a basin can differ between small and large rainfall depths and intensities. Sivapalan et al. (1990) used the Philip (1957) equation to simulate infiltration-excess runoff and an analytical soil moisture deficit equation to simulate saturation-excess runoff for hypothetical basins. They found that saturation-excess runoff is dominant for floods with return periods less than 20 years and infiltration-excess runoff dominates for storms with return periods more than 100 years. Dunne and Black (1970b) performed a study on a Vermont hillslope and found that subsurface stormflow comprises the hydrograph for storms with return periods less than two years, while saturation-excess runoff occurs for storms with return periods ranging from three years to several hundred years.

Changes in the streamflow production mechanism can also lead to nonlinearities in the basin's response to storm events. Sivapalan et al. (1990) determined that the shape of the flood frequency curve depends on whether infiltration-excess or saturation-excess runoff dominates. Kusumastuti et al. (2007) conducted model simulations with and without a limited soil storage capacity and determined that including the storage limitation produces a streamflow peak late in the storm (when the capacity is exceeded) that is not observed with the infinite capacity model. Additionally, they showed the change in the dominant mechanism from subsurface stormflow to saturation-excess runoff creates an inflection point in the flood frequency curve.

Only a few studies have directly analyzed the active runoff mechanisms for large storms in forested regions. Dunne and Black (1970) observed various natural and simulated storms with return periods up to several hundred years in the humid Sleepers River watershed in Vermont. They found that outflow was dominated by saturation-excess runoff, and rainfall intensities were never large enough to produce infiltration-excess runoff. Troch et al. (1994) used the model developed by Sivapalan et al. (1990) for 12 flood events in a small watershed in central Appalachia with return periods ranging from one to 23 years, including the highest peak flow on record during tropical storm Agnes. Saturation-excess runoff produced greater than 80% of the total runoff for 11 of the 12 events and 100% of total runoff for five of the 12 events. Sturdevant-rees et al. (2001) used Richards equation to determine that both saturation-excess and infiltration-excess runoff occurred in central Appalachia during Hurricane Fran for which streamflow return periods exceeded 100 years. However, no known studies have considered the active streamflow production mechanisms for extreme events in western U.S. mountains. These forested watersheds have a much different climate than the Appalachians. They have less exposure to hurricanes (Colorado Division of Water Resources and New Mexico Office of the State Engineer 2018) and transition from Steppe climate at lower elevations to cold regions without a dry season at higher elevations (Peel et al. 2007).

The objectives of this study are to (1) determine the streamflow production mechanisms that were active for large historical storms in the Colorado Front Range, (2) determine the mechanisms that are active for design storms used in hydrologic evaluations and whether current guidelines are sufficient to simulate these mechanisms, and (3) propose modeling methods to simulate these mechanisms that can be readily used by consultants for hydrologic evaluations. Three large historical events with available data are modeled for the five basins (Figure 1.1). The two events discussed in detail are the September 2013 event in SBC and the July-August 1976 event in the North Fork Big Thompson River basin (NFBTR). These two events were selected because they are among the largest floods on record in the Colorado Front Range and were produced by different types of storms. HEC-HMS is used to simulate the events because it is widely used by consultants for hydrologic analyses and has methods that can simulate the infiltration-excess, saturation-excess, and subsurface stormflow mechanisms. After analyzing the historical events, the models are also applied for several design storms.

The outline of this report is as follows. Section 2 provides background about the Colorado Front Range and the historical storm events that were modeled. Section 3 discusses the modeling methods used to investigate the runoff mechanisms. Section 4 presents the model results for both the historical and design

storms, and Section 5 summarizes the main conclusions. Appendix A provides a more detailed explanation of the pre-processing of the model forcing data and the parameter estimation process that was used to construct the models. Appendices B through D provide scripts that automate portions of the pre-processing and parameter estimation process.
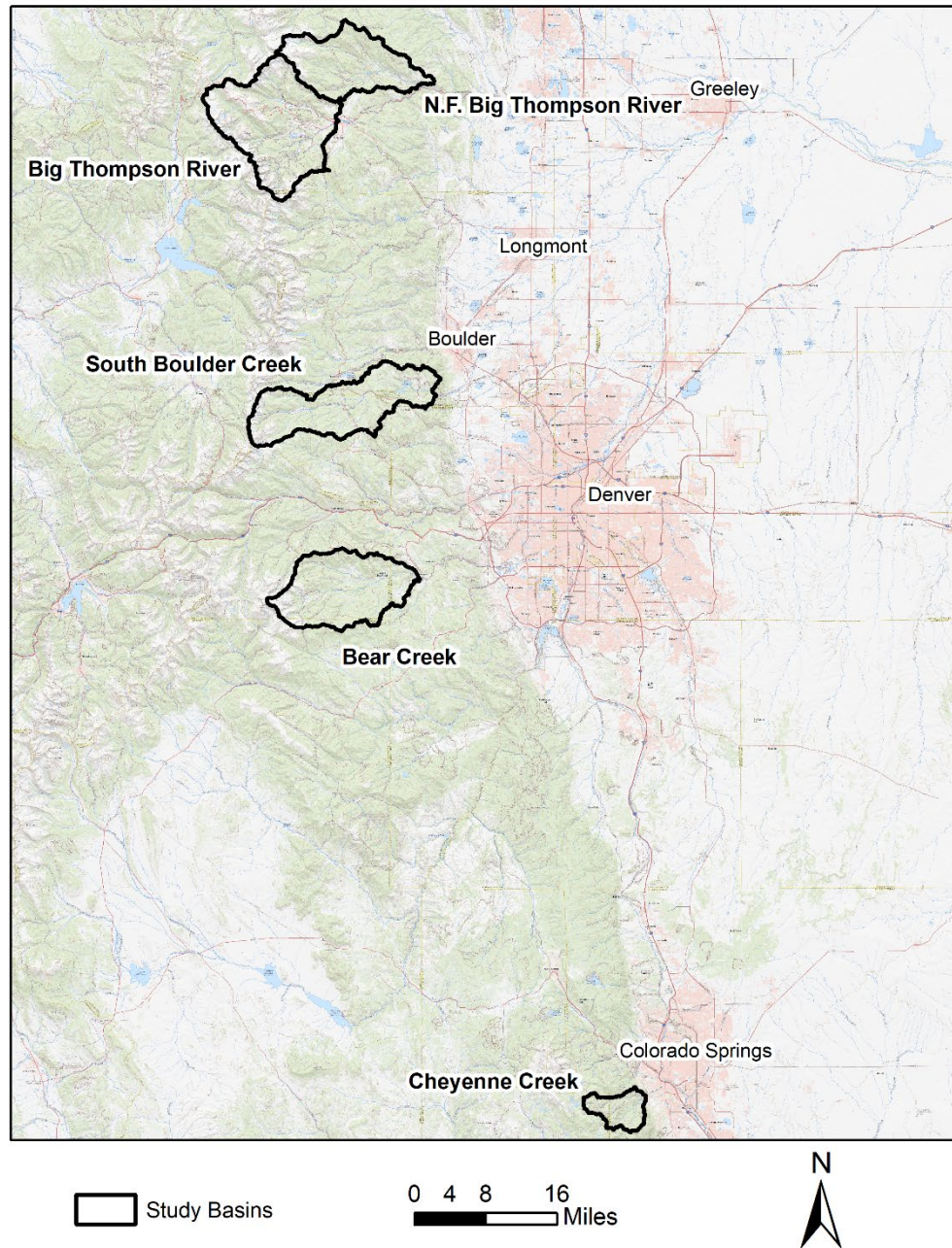
Figure 1.1 Locations of study basins throughout the Colorado Front Range

2. STUDY REGION AND EVENTS

The climate of the Front Range is typically classified as arid to semiarid at lower elevations and humid or tundra at higher elevations (Greenland et al. 1985). Floods at lower elevations are typically rainfall-induced, while floods at higher elevations usually derive from snowmelt (Jarrett and Costa 1988). Four types of flood-producing rainfall events occur in Colorado: local storm (LS), mesoscale with embedded convection (MEC), mid-latitude cyclone (MLC), and tropical storm remnant (TSR) (Colorado Division of Water Resources and New Mexico Office of the State Engineer 2018). An LS is defined as a small-scale convective event that occurs from April through October with a spatial extent of less than 100 mi^2 and a duration of one hour or less. An MEC is also a warm-season thunderstorm but has a spatial extent up to 1,000 mi^2 and a duration of about six hours. An MLC is a large, synoptic-scale low-pressure system with cyclonic circulation that forms in the mid-latitudes, and it typically occurs in the cool season from November through March. An MLC can produce precipitation for several days over very large areas. Finally, a TSR results directly from a tropical cyclone or hurricane, can occur from June through October, and has a comparable size and duration to MLCs.

Vegetation and soil properties in the Front Range depend on aspect, particularly at lower elevations (Anderson et al. 2011). South-facing slopes (SFS) receive more solar radiation than north-facing slopes (NFS) (Anderson et al. 2014). Thus, SFS experience snow-free periods in winter as snow typically melts between storms, while NFS experience more severe and longer freezing and often maintain snow until spring (Anderson et al. 2014). Similarly, soils on NFS become wet in the spring and stay wet for long periods, while soils on SFS undergo more frequent wetting events of shorter duration (Coleman and Niemann 2013; Anderson et al. 2014). Because of these climatic differences, NFS are densely vegetated with lodgepole pine, aspen, Rocky Mountain Douglas fir, and limber pine with little understory. SFS are sparsely vegetated with trees, shrubs, and grassy and herbaceous understory (Anderson et al. 2011; Ebel 2013). The climatic and vegetation differences between hillslopes have also produced differences in weathering and soil properties. NFS have a thicker weathered soil horizon and higher organic content (Anderson et al. 2014).

An MLC event occurred throughout the Front Range from September 9, 2013, to September 16, 2013, when a large-scale atmospheric flow pattern transported abnormally high atmospheric moisture from the Gulf of Mexico and Pacific Ocean to the Front Range where it was held in place by an anticyclone to the north (Gochis et al. 2015). Total rainfall depths exceed 380 mm in some locations over an eight-day period (National Weather Service and NOAA 2013). Peak streamflows exceeded the 200-year event at five gauges and the 100-year event at 11 gauges in the Front Range (Yochum 2015). The flooding caused eight deaths and over \$2 billion in damage (Gochis et al. 2015). The 2013 storm is modeled for SBC with an outlet at the Colorado Division of Water Resources (DWR) stream gauge South Boulder Creek near Eldorado Springs, CO (BOCELSCO). The drainage area at the gauge is 278 km^2, and the basin elevation range is 1,900 – 4,050 m. The river stage exceeded the existing rating curve during the storm, but DWR extrapolated the curve to estimate the discharges at higher stages. The peak streamflow during the storm exceeded the 100-year event by a ratio of 1.6 (Capesius and Stephens 2009). The basin includes Gross Reservoir and the South Boulder Creek Diversion, which diverts water out of the basin downstream of Gross Reservoir. It also includes Moffat Tunnel, which diverts water into the basin in its headwaters. The 2013 storm was also modeled for Bear Creek at Evergreen (BCREVRCO) (267 km^2), Big Thompson River above Lake Estes (BTABESCO) (357 km^2), and Cheyenne Creek at Colorado Springs (CHEEVACO) (56 km^2), although these results are not discussed in detail.

A MEC event occurred in the Big Thompson watershed from July 31, to August 1, 1976, when a moist unstable airmass was pushed into the Rocky Mountains where uplift enhanced convection (McCain et al. 1979). Southeasterly winds held the storm stationary over the foothills while over 300 mm of rainfall fell within a 50-hour period. Much of the rainfall accumulation occurred within a three-hour period (McCain et al. 1979). Peak flows for the Big Thompson River exceeded the 100-year event by a ratio of 1.8 at the canyon mouth and by a ratio of 3.8 at the town of Drake where the NFBTR connects to the main stem (McCain et al. 1979). As a result of the flooding, 139 deaths occurred and damage exceeded $35 million (McCain et al. 1979). Due to data availability, the 1976 event is modeled for NFBTR with its outlet at the DWR gauge North Fork Big Thompson River at Drake, CO (BTNFDRCO). The drainage area at the gauge is 220 km^2, and the basin's elevation range is 1,875 – 4,150 m. The streamflow data for this event are incomplete because the gauge became plugged with sediment, but the peak streamflow was captured (McCain et al. 1979).

A smaller MLC event from June 1997 is modeled for Cheyenne Creek with its outlet at the DWR gauge Cheyenne Creek at Colorado Springs (CHEEVACO). The drainage area at the gauge is 56 km^2, and the basin's elevation range is 1,905-3,770 m. Rainfall lasted about 36 hours, and the total rainfall depth was approximately 120 mm (Applied Weather Associates 2018). The ratio of the 1997 peak discharge to the 100-yr streamflow is approximately 0.4 (Capesius and Stephens 2009). No information is available about loss of life or property damage for the storm, and the results from this event are not discussed in detail due to its smaller size.

In addition to these historical events, design storms are considered for all the basins. The design storms include 10^{-3}, 10^{-4}, 10^{-5}, 10^{-6}, and 10^{-7} annual exceedance probability (AEP) events and the PMP. These storms were selected because they are used in Colorado's dam safety guidelines (Colorado Division of Water Resources and New Mexico Office of the State Engineer 2018).

3. MODELING METHODOLOGY

3.1 Rainfall Input

The spatial and temporal rainfall patterns for the historical storms were obtained from the Storm Precipitation Analysis System (SPAS). SPAS has been used to analyze over 500 extreme precipitation events and has demonstrated reliability in post-storm analyses (MetStat 2018). SPAS uses base maps of climate variables and observations from rain gauges (in addition to NEXRAD data for storms since the mid-1990s) to estimate the spatial distribution of rainfall between gauges (MetStat 2018). The analysis for the September 2013 storm used 2,635 rain gauges, while the analysis for the 1976 storm includes 119 rain gauges. The final product from SPAS was provided to the study authors as gridded rainfall depths with a temporal resolution of 60 min and a spatial resolution of 2,000 m for SBC and 36 arc-seconds (approximately 850 m x 1,100 m) for the remaining basins. Figure 3.1 shows the spatial pattern of total rainfall depth for each basin that was modeled. Noteworthy spatial variation exists during the 2013 storm in SBC with the heaviest rainfalls occurring near the outlet (Figure 3.1a). This storm is more homogeneous for the Big Thompson River (Figure 3.1c), Bear Creek (Figure 3.1d), and Cheyenne Creek (Figure 3.1e). The rainfall for the 1976 event is localized over the central portion of the NFBTR basin (Figure 3.1b).

Rainfall data for the design storms were obtained from the Colorado-New Mexico Regional Extreme Precipitation Study (DWR and New Mexico Office of the State Engineer 2018), which replaced the National Oceanic and Atmospheric Administration's (NOAA) hydrometeorological report for this region.

3.2 Model Structure

3.2.1 Disaggregation of Sub-basins

A semi-distributed model was constructed for each basin in HEC-HMS. HEC-HMS considers very limited aspects of spatial variability within each sub-basin, so the number of sub-basins is an important consideration in model development. Previous studies have shown that the most important criteria in determining the level of basin disaggregation is capturing the spatial variation of rainfall (Andréassian et al. 2004; Zhang et al. 2004).

The disaggregation process used in this study was described in detail by Djokic et al. (2011) and has been implemented in a number of other studies (Comair et al. 2012; Li 2014). The process begins with a digital elevation model (DEM), which in this case has a resolution of 1/3 arc-second and was obtained from the National Elevation Dataset. A contributing area threshold is specified that determines where the channels begin. A sub-basin is then created for each link in the resulting channel network. A smaller threshold results in a more extensive network and more sub-basins. Because each sub-basin can receive different rainfall data, increasing the number of sub-basins typically improves the model's representation of spatial rainfall variation. Adequate basin disaggregation is achieved when the spatial variation of rainfall within each sub-basin is relatively small, and the number of sub-basins is still manageable for modeling purposes (Zhang et al. 2004).

To evaluate different levels of basin disaggregation, the coefficient of variation (COV) of total storm depth within each sub-basin was calculated and averaged for all sub-basins using thresholds from 4 km^2 to 35 km^2 (Figure 3.2). Figure 3.2a shows a clear reduction in COV between thresholds of 22 km^2 and 15 km^2 for SBC. Below 15 km^2, further improvement is not achieved until 6 km^2. However, the number of sub-basins increases from 11 at 15 km^2 to 35 at 6 km^2 (Figure 3.2b). The other basins for which the 2013

storm was modeled show more steady reductions in the average COV. For NFBTR (1976 storm), substantial variation remains even with very small thresholds, and the number of sub-basins becomes very large. From these results, a threshold of 15 km^2 was selected. Figure 3.1 shows the sub-basin configurations for each model when the 15 km^2 threshold is used. The number of sub-basins in the models ranges from 3 to 15. Figure 3.1b also shows why the COV is large for the NFBTR case. Large rainfall depths are concentrated at the downstream ends of the headwater sub-basins, and these sub-basins are not readily divided by decreasing the channel threshold.

The sub-basins are then further divided into NFS and SFS elements to account for the variation in the vegetation and soil properties between the opposing hillslopes. Dividing the hillslopes into separate modeling units and adding their responses at the sub-basin outlet relies on the linear behavior of unit hydrograph theory (i.e., flows are additive) (Sherman 1932). Figure 3.3 shows the HEC-HMS model structure that results from the disaggregation of each basin.

3.2.2 Process Representation

The following processes are included in the models: canopy (interception by vegetation), loss (infiltration and streamflow generation), transform (conversion of excess rainfall to streamflow at each sub-basin outlet), and routing (flow through channels to the basin outlet). The methods used to represent these processes are: (1) canopy: simple canopy, (2) loss: soil moisture accounting (SMA), (3) transform: Clark Unit Hydrograph, and (4) Routing: Muskingum-Cunge with eight-point cross section. In addition, for SBC, a Reservoir, Source, and Diversion are also included to account for the water infrastructure in the basin.

The simple canopy method is used to represent the vegetation canopy because it can adequately simulate interception and has simple parameter requirements. SMA is used because it can simulate infiltration-excess and saturation-excess runoff. One groundwater layer (GW 1) and an associated linear reservoir are also included in SMA to simulate subsurface stormflow. Baseflow is not simulated. Figure 3.4 shows the SMA storage elements and the pathways by which water can move between these elements (Feldman 2000). The Clark method is used because it can account for noncontiguous NFS and SFS with customized time-area curves. Muskingum-Cunge is used for routing because it is the only method currently available in HEC-HMS that allows overbank flows (Feldman 2000), which are expected to be important for extreme events. It is also applicable for a wide range of channels because it accounts for lag and attenuation, and it accepts physical characteristics as its parameters (Feldman 2000).

3.3   Model Parameters

3.3.1 Canopy Method

All rainfall fills the canopy storage until it reaches the specified maximum storage. If the canopy storage is full, additional rainfall becomes throughfall. Storage in the canopy layer depletes at a specified potential evapotranspiration (PET) rate. The required parameters are the initial canopy storage, maximum canopy storage, and the PET rate.

The maximum canopy storage and PET rate were estimated based on throughfall measurements taken in the Cache la Poudre catchment during the 2013 storm (Traff et al. 2015). The catchment included three rain gauges on NFS and two on SFS. Two of the NFS gauges were under ponderosa pine canopy (which is common on NFS at lower elevations in the Front Range), while one was in the open. One SFS gauge was located under antelope bitterbrush canopy (which is common on SFS at lower elevations in the Front Range), while one was in the open. The Simple Canopy model was implemented for the catchment

7

hillslopes, and the maximum canopy storage and PET rate were calibrated to optimize the Nash-Sutcliffe Coefficient of Efficiency of the modeled throughfall as compared with the observed throughfall. The calibrated PET rate likely includes both evapotranspiration and stemflow to the ground surface. Both processes drain the canopy over time and should be included in the model, but the calculated PET rate should be interpreted as a canopy depletion rate rather than a true PET rate. This analysis also assumes the gauges in the Cache la Poudre catchment are representative of the Front Range because the resulting parameters are used directly for all basins. While this assumption introduces error in the model results, no additional throughfall data were found for large storms in the Front Range.

3.3.2 Loss Method

SMA was originally developed based on the Precipitation-Runoff Modeling System (Leavesley et al. 1983; Feldman 2000). In SMA, the soil's infiltration capacity is calculated as a linear function of the current soil storage (Figure 3.5a). The line is defined by the maximum soil storage and maximum infiltration rate parameters. The actual infiltration rate is then calculated as the smaller of the infiltration capacity and the throughfall. While this model is conceptual, it can simulate both infiltration-excess and saturation-excess runoff. If the maximum soil storage parameter is very large, runoff only occurs when the rainfall rate exceeds a non-zero infiltration capacity (Figure 3.5b). Thus, the model is similar to a uniform loss method, and runoff occurs by the infiltration-excess mechanism. If, instead, the maximum infiltration rate parameter is very large, runoff only occurs when the soil layer completely saturates, which produces saturation-excess runoff (Figure 3.5c).

In this study, the maximum infiltration rate and maximum soil storage are estimated from basin properties, so both mechanisms are possible. Runoff is considered saturation-excess if the saturated fraction is above 85%. When the saturated fraction is that high, the infiltration capacity is below 15% of the maximum infiltration rate. This value is smaller than what would occur due to an infiltration-excess mechanism. For example, the asymptotic infiltration capacity in the Horton model is usually estimated as 20% of the initial infiltration (Viessman and Lewis 2003).

Evapotranspiration from the soil layer is neglected because this study focuses on single events, and evapotranspiration is small over short periods. Water leaves the soil layer and enters the GW 1 layer through soil percolation. The soil percolation rate is calculated as a function of the maximum soil percolation rate parameter and the current storages of the soil and GW 1 layers (Feldman 2000). The GW 1 layer represents the saturated layer of weathered bedrock on top of the intact bedrock. Water can leave the GW 1 layer through subsurface stormflow and deep percolation. Subsurface stormflow exits the GW 1 layer as a linear function of the GW 1 storage, which requires specification of the GW 1 storage coefficient and maximum GW 1 storage parameters. Subsurface stormflow is then routed through a linear reservoir, which requires the linear reservoir storage coefficient parameter. The reservoir outflow becomes part of the streamflow at the sub-basin outlet. Deep percolation is calculated as a linear function of the groundwater storage and requires specification of the GW1 maximum percolation parameter. This water does not enter the streams.

The maximum infiltration parameter was estimated based on the Green and Ampt (1911) model, which calculates the infiltration capacity f as:

$$f = K_{sat}\left[1 + \frac{|\psi_f|}{\delta}\right]$$

(1)

where K_{sat} is the saturated hydraulic conductivity, ψ_f is the wetting front suction head, and δ is the depth of the wetting front at the time of interest. The maximum infiltration capacity occurs immediately after ponding, but the depth of the wetting front at this time depends on the rainfall rate and soil properties

8

(Chow et al. 1988). δ was selected to be 76 mm based on realistic ranges for rainfall rates and soil properties in the region, and the associated f was used for the maximum infiltration parameter. To calculate f, the percent sand, clay, and organic matter in the top 457 mm of soil were obtained as gridded data from the Soil Survey Geographic (SSURGO) database (Soil Survey Staff 2019). This depth was obtained from Colorado's existing guidelines for storms with return periods of 100-year or larger and reflects the anticipated wetting front depths for such events (Sabol 2008). The soil property grids were then used in pedotransfer functions (Rawls et al. 1983; Saxton and Rawls 2006) to calculate grids of bare soil K_{sat} and ψ_f. The bare soil K_{sat} was then adjusted using vegetation cover because vegetation prevents soil crusting and increases infiltration (Rawls et al. 1989; Sabol 2008). Fractional vegetation was calculated for each cell based on the normalized difference vegetation index (Montandon and Small 2008; Vermote et al. 2016). K_{sat} was divided by two because the effective hydraulic conductivity for unsaturated flow is approximately half the value for saturated flow (Bouwer 1964). Once the maximum infiltration grid was determined, spatial average values were calculated for each NFS and SFS sub-basin.

The maximum soil storage was calculated as the available pore space in the soil. Porosity grids were calculated from the gridded percent sand, clay, and organic matter and pedotransfer functions (Rawls et al. 1983; Saxton and Rawls 2006). The depth to restricting layer was obtained directly from SSURGO. The average porosity and depth to restrictive layer were then calculated for each NFS and SFS sub-basin, and those two variables were multiplied to obtain the maximum soil storage.

The initial soil storage is input in the model as a percent of the total storage initially filled. It was estimated for the 1997 and 2013 storms using the Mosaic model's soil moisture (0 – 100 mm depth) in the North American Land Data Assimilation System (NLDAS) (Xia et al. 2012). Because NLDAS data were not available for 1976, the initial soil storage for this storm was assumed to be at field capacity per recommendations from existing guidelines for normal antecedent conditions (Sabol 2008). Field capacity soil moisture was calculated from soil textures and pedotransfer functions (Rawls et al. 1983; Saxton and Rawls 2006).

The maximum soil percolation rate was determined from saturated hydraulic conductivity measurements for weathered bedrock in the Front Range. The measurements were collected at the Sugarloaf experimental catchment using a tension infiltrometer (Ebel 2016). The average value of the measurements was applied uniformly for all models. Additional measurements would be helpful, but no other saturated hydraulic conductivity data for weathered bedrock were found for the Front Range.

The storage coefficients for the GW 1 layer and reservoir were estimated based on a hydrograph recession analysis of the largest storms with available data for each basin (Linsley et al. 1958; Fleming and Neary 2004). A June 2003 storm was used for SBC; a May 1999 storm was used for NFBTR; and the September 2013 storm was used for the remaining basins. The September 2013 storm was not used for SBC because the available dataset does not include the entire recession. The hydrograph was assumed to comprise surface flow, subsurface flow, and baseflow. The exponential linear reservoir recession equation was used to determine the baseflow, and baseflow was removed from the hydrograph. The subsurface stormflow forms the recession of the remaining hydrograph, so another exponential linear reservoir equation was then fit to the recession to characterize subsurface stormflow. Because subsurface stormflow is routed through two linear reservoirs in SMA, the exponential equation for two linear reservoirs in series (Nash 1957) was used to characterize subsurface stormflow. The storage coefficients for the two reservoirs were assumed to be the same, and the calculated values were applied uniformly to all sub-basins. The maximum storage that occurred during each storm was also obtained from the analysis. This value gives an indication of the minimum value that could be used for the maximum GW 1 storage parameter; however, this parameter was primarily determined from calibration. The GW 1 maximum percolation is also determined from calibration.

3.3.3 Direct Flow Transform

The Clark unit hydrograph method uses a cumulative time-area curve to account for the translation of flow to the sub-basin outlet and a linear reservoir to account for storage effects (Clark 1945). The method requires specification of a dimensionless cumulative time-area curve, the time of concentration T_c (which rescales the provided curve), and a storage coefficient R for the linear reservoir (Feldman 2000).

The dimensionless time-area curve for each NFS and SFS sub-basin was calculated based on the DEM and Manning's Equation. Each DEM grid cell was identified as either a channel or hillslope using a contributing area threshold. The threshold was selected to obtain channel extents that approximate the flow lines from the National Hydrography Dataset (U.S. Geological Survey National Geospatial Program 2018) and streams observed in satellite imagery. Channel cross-sections were assumed to be rectangular for simplicity, and the dimensions were estimated using relationships that relate bank-full width and depth to contributing area for the Front Range (Livers and Wohl 2015). Manning's roughness was determined based on representative values for landcover types (Chow 1959), which were obtained from the National Land Cover Dataset 2011 (Follum et al. 2017). Hillslope cell travel times were calculated using an approximation of Manning's equation that combines the hydraulic radius and roughness coefficient into a constant factor. The factor was estimated based on values developed for forested and woodland regions by McCuen (1989). The total travel time to the sub-basin outlet was then calculated by starting at all locations in the sub-basin of interest (either NFS or SFS) and summing the cell travel times along the flow path to the outlet. The longest travel time to the outlet was used as the time of concentration. The linear reservoir's storage coefficient was calculated using an empirical equation from Colorado's current hydrology guidelines that depends on the time of concentration (Sabol 2008).

3.3.4 Channel Routing

Muskingum-Cunge is a diffusion wave routing method that improves upon the Muskingum model in part because its parameters are physical characteristics (Feldman 2000). In HEC-HMS, the method requires the channel length, channel slope, roughness coefficients for the floodplain and channel, a reference flow, and the cross-section geometry of the floodplain and channel. The reference flow is the value at which the Muskingum-Cunge approximation is exact, and the approximation becomes less accurate farther from the reference (Feldman 2000).

Floodplain dimensions were estimated using the DEM. Up to four valley cross-sections were analyzed along each reach, and a representative cross-section was selected. Channel widths were estimated from satellite imagery, and channel depths were calculated using Manning's equation to find the flow depth for the bank-full discharge in the channel. The bank-full discharge was estimated as the two-year flow rate from StreamStats.

The reference flow was estimated as half of the observed peak flow during the modeled storm. Additional simulations were run using the bank-full flow as the reference flow, and the change had very little impact on the model results. Roughness coefficients were estimated using representative values for the observed channel type, vegetation, and substrate (Chow 1959), which were estimated based on satellite imagery.

3.3.5 Reservoir Routing

Reservoir routing is needed to describe the behavior of Gross Reservoir. An elevation-storage curve, specifications of the reservoir's outlet structures, and an initial condition were specified in the model. All

of the reservoir routing parameters were obtained from DWR and Denver Water, which operates this reservoir.

3.3.6 Sources and Diversions

The addition of water from Moffatt Tunnel and the loss of water from the South Boulder Creek Diversion were also included in the SBC model. Flow data for both diversions were provided by DWR, which maintains a network of stream gauges throughout Colorado.

3.3.7 Parameter Summary

Tables 3.1 to 3.10 provide the model parameters for the study basins. Parameters that vary by sub-basin are provided in the first table for each basin, and parameters that are constant for all sub-basins within a given basin are shown in the second table. Bear Creek has an average maximum soil storage of 309 mm among its sub-basins, which is substantially larger than the other basins. Cheyenne Creek has the lowest maximum soil storage, averaging 148 mm across its sub-basins. These values indicate that saturation-excess runoff might be rarer for Bear Creek and more common for Cheyenne Creek. The Big Thompson River has the lowest maximum infiltration rates, averaging 40 mm/hr across its sub-basins. Cheyenne Creek has the highest maximum infiltration rates with an average of 58 mm/hr. Thus, infiltration-excess runoff is expected to occur at lower rainfall intensities for the Big Thompson River basin than the Cheyenne Creek basin. Maximum infiltration rates recommended in current Colorado guidelines are substantially lower as they typically range from 0.5 mm/hr to 10 mm/hr (Sabol 2008). The ratio $R / (T_c + R)$ has been found to be fairly consistent for basins within a given region (Dunn et al. 2001; FERC 2001). Dunn et al. (2001) optimized R and T_c for 30 gauged sub-basins in the Sacramento River and San Joaquin River watersheds and determined ratios between 0.6 and 0.8. Wilkerson and Merwade (2010) calculated R and T_c values for basins within three regions of Indiana. The resulting ratios range from 0.13 to 0.72. For the Front Range basins in the present study, the average ratio within each basin ranges from 0.40 to 0.47.

3.3.8 Calibration

A limited calibration was performed for parameters that have substantial uncertainty in their estimates and a significant impact on the model results. These parameters include the maximum soil storage, maximum infiltration rate, time of concentration, Clark storage coefficient, and all GW 1 parameters. Because automatic calibration techniques often perform poorly for models with many parameters (Boyle et al. 2000), the calibrations were performed manually. Each initial parameter estimate was multiplied by a uniform calibration factor for all sub-basins. The calibration factors were constrained so the calibrated parameters remain within physically realistic ranges. Performance metrics used in the calibration include Nash-Sutcliffe Coefficient of Efficiency (NSCE), peak flow error, and visual goodness-of-fit.

Table 3.11 provides the calibration factors for each parameter in each basin. The calibration factor for soil storage is always less than one, suggesting the values derived from SSURGO overestimate the available storage in these Front Range basins. The calibration factors for time of concentration are greater than one for SBC, Big Thompson River, and Cheyenne Creek, indicating the runoff takes longer than expected to reach the sub-basin outlets. However, the calibration factor for the 1976 storm in NFBTR is 0.05. The 1976 storm had peak rainfall intensities above 90 mm/hr in some locations, while the 2013 storm had peak intensities between 18 and 35 mm/hr. Higher rainfall intensities might lead to greater flow depths, which would reduce the effects of friction and produce higher velocities. To analyze the effect of rainfall intensity on the travel times, the time of concentration was estimated as a function of

effective rainfall intensity following (Eagleson 1970). The ratio of the time of concentration for the flood event and bank-full flow was then estimated. The ratio is approximately 0.4 for the 1976 storm, and it ranges from 1.0 to 2.9 for the 2013 storm. Thus, the difference in rainfall intensity may partially explain the calibration factors. The rainfall pattern for the 1976 storm may also help explain the calibration factors for time of concentration. The largest rainfall depths were concentrated at the downstream end of the five headwater basins (Figure 3.1b). In the model, the rainfall is assumed to occur uniformly across each sub-basin, so it assumes longer flow distances than occurred in reality.

Substantial uncertainty occurs in the hydrograph recession analysis that was used to estimate the subsurface stormflow parameters. Because the analysis only provides the maximum GW 1 storage that occurred during the analyzed events, calibration is required to determine the GW 1 maximum storage parameter. The final values range from 0.3 – 4.0 mm. The GW 1 storage coefficient is also substantially decreased in the calibration process. The GW 1 maximum percolation was calibrated so that NFS have higher percolation rates than SFS (Anderson et al. 2014).

Table 3.1 Model parameters for South Boulder Creek that vary by sub-basin

Sub-Basin	Aspect	Max Soil Storage (mm)	Initial Soil Storage (%)	Max Infiltration Rate (mm/hr)	Clark UH T_c (hr)	Clark UH R (hr)
1	South	249.84	6	62.97	6.4	11.4
1	North	274.43	6	56.41	6.5	11.6
2	South	280.71	6	54.26	4.6	11.2
2	North	255.44	6	56.73	4.6	9.2
3	South	374.88	4	57.61	7.3	13.1
3	North	411.73	4	62.25	7.0	13.7
4	South	239.59	6	68.03	5.6	12.5
4	North	272.36	6	73.77	5.7	15.2
5	South	265.83	6	52.02	6.1	9.6
5	North	253.83	6	56.51	6.1	6.8
6	South	227.71	7	51.76	5.2	11.5
6	North	217.28	8	58.54	5.1	8.1
7	South	216.42	8	39.26	4.4	15.2
7	North	239.86	7	42.48	4.3	16.3
8	South	304.2	5	48.16	6.2	9.5
8	North	276.41	6	51.57	6.2	9.4
9	South	190.13	9	40.34	7.9	10.7
9	North	246.81	7	47.79	7.9	8.0
9b	South	244.79	7	43.61	7.5	17.1
9b	North	253.46	7	46.95	7.4	16.9
10	South	232.35	7	42.53	4.9	9.4
10	North	253.68	7	45.93	5.0	11.1
11	South	98.59	14	47.09	4.6	6.9
11	North	127.24	11	53.83	4.5	7.0

Table 3.2 Model parameters for South Boulder Creek that are constant for all sub-basins

Aspect	Max Canopy Storage (mm)	Max Soil Percolation (mm/hr)	GW 1 Max Storage (mm)	GW 1 Storage Coefficient (hr)	L.R. GW 1. Storage Coefficient (hr)
South	1.5	82.9	10.5	11.7	11.7
North	7.2	82.9	10.5	11.7	11.7

Table 3.3 Model parameters for North Fork Big Thompson River that vary by sub-basin

Sub-Basin	Aspect	Max Soil Storage (mm)	Initial Soil Storage (%)	Max Infiltration Rate (mm/hr)	Clark U.H. T_c (hr)	Clark U.H. R (hr)
1	South	180.6	7.7	61.9	0.65	7.96
1	North	160.2	7.6	64.8	0.65	7.82
2	South	158.1	6.6	59.1	0.35	2.24
2	North	192.0	6.6	62.4	0.36	3.64
3	South	220.7	7.5	53.3	0.41	3.86
3	North	238.2	7.4	61.5	0.42	3.71
4	South	144.6	7.0	56.6	0.37	3.86
4	North	148.2	7.4	59.6	0.34	3.68
5	South	130.4	6.7	50.8	0.25	2.38
5	North	186.3	6.5	58.5	0.25	2.21
6	South	187.8	7.9	58.7	0.04	0.59
6	North	211.5	5.4	74.4	0.02	0.55
7	South	217.0	6.2	70.4	0.38	2.45
7	North	201.2	6.2	76.1	0.38	3.80
8	South	177.8	6.6	56.2	0.24	3.02
8	North	191.0	6.6	66.1	0.25	2.33
9	South	165.5	6.6	56.8	0.30	1.69
9	North	188.8	6.6	60.5	0.30	2.10

Table 3.4 Model parameters for North Fork Big Thompson River that are constant for all sub-basins

Aspect	Max Canopy Storage (mm)	Max Soil Percolation (mm/hr)	GW 1 Max Storage (mm)	GW 1 Storage Coefficient (hr)	L.R. GW 1. Storage Coefficient (hr)
South	1.5	82.9	0.57	19.5	19.5
North	7.2	82.9	0.57	19.5	19.5

Table 3.5 Model parameters for Bear Creek that vary by sub-basin

Sub-Basin	Aspect	Max Soil Storage (mm)	Initial Soil Storage (%)	Max Infiltration Rate (mm/hr)	Clark U.H. T_c (hr)	Clark U.H. R (hr)
1	South	52.5	3.2	44.1	9.37	7.60
1	North	53.9	3.1	47.2	8.65	5.54
2	South	36.5	4.2	55.3	6.09	5.89
2	North	47.5	3.2	72.4	6.12	3.18
3	South	49.8	2.2	41.9	2.13	1.68
3	North	69.6	3.3	70.7	2.13	1.24
4	South	42.7	4.8	57.7	4.86	2.83
4	North	47.5	4.1	62.8	4.89	3.38
5	South	38.1	5.5	51.8	1.39	1.51
5	North	46.6	4.5	61.4	1.43	3.06
6	South	40.0	3.9	51.8	4.91	5.39
6	North	57.2	5.5	62.9	4.38	2.70
7	South	66.9	3.2	49.2	3.47	1.77
7	North	78.9	2.6	58.0	3.68	3.68
8	South	55.3	3.1	45.2	3.56	3.37
8	North	60.2	2.7	51.3	3.72	3.72
9	South	41.4	5.6	40.4	1.47	1.92
9	North	32.8	7.0	44.5	1.30	1.48

Table 3.6 Model parameters for Bear Creek that are constant for all sub-basins

Aspect	Max Canopy Storage (mm)	Max Soil Percolation (mm/hr)	GW 1 Max Storage (mm)	GW 1 Storage Coefficient (hr)	L.R. GW 1. Storage Coefficient (hr)
South	1.5	82.9	0.02	22.8	22.8
North	7.2	82.9	0.02	22.8	22.8

Table 3.7 Model parameters for Big Thompson River that vary by sub-basin

Sub-Basin	Aspect	Max Soil Storage (mm)	Initial Soil Storage (%)	Max Infiltration Rate (mm/hr)	Clark U.H. T_c (hr)	Clark U.H. R (hr)
1	South	157.9	3.6	40.4	15.8	8.4
1	North	150.5	3.9	43.3	15.6	8.6
2	South	173.8	8.0	37.3	9.2	5.9
2	North	104.2	6.6	37.1	10.8	5.6
3	South	173.8	4.6	36.9	19.0	10.4
3	North	186.3	4.3	38.9	19.2	10.9
4	South	158.6	4.8	38.4	19.0	10.4
4	North	157.5	5.0	41.5	13.4	6.4
5	South	109.0	8.6	41.5	8.5	5.1
5	North	91.4	10.3	45.9	8.7	2.9
6	South	98.4	9.5	33.3	2.5	5.4
6	North	254.0	3.7	44.4	1.3	4.1
7	South	95.8	9.8	32.8	6.5	5.4
7	North	101.6	9.2	41.2	6.5	4.3
8	South	88.6	7.7	36.3	7.6	4.8
8	North	145.2	5.3	38.1	7.3	6.9
9	South	75.2	11.6	35.2	8.7	5.5
9	North	127.6	7.3	39.2	7.5	5.1
10	South	61.9	9.0	36.9	9.8	5.6
10	North	67.7	8.2	36.8	9.8	8.6
11	South	149.3	3.8	38.2	11.1	4.5
11	North	113.4	5.0	37.7	11.2	4.7
12	South	132.4	3.8	37.5	13.9	10.0
12	North	136.3	3.9	43.0	13.3	8.6
13	South	276.7	1.9	34.7	2.0	2.7
13	North	204.5	3.6	40.4	1.6	1.7
14	South	100.6	4.8	39.1	8.7	7.1
14	North	82.3	5.9	41.1	9.0	11.0
15	South	177.3	2.8	30.4	3.5	5.0
15	North	192.6	2.8	33.1	4.0	7.3

Table 3.8 Model parameters for Big Thompson River that are constant for all sub-basins

Aspect	Max Canopy Storage (mm)	Max Soil Percolation (mm/hr)	GW 1 Max Storage (mm)	GW 1 Storage Coefficient (hr)	L.R. GW 1. Storage Coefficient (hr)
South	1.5	82.9	0.0001	5	5
North	7.2	82.9	0.0001	5	5

Table 3.9 Model parameters for Cheyenne Creek that vary by sub-basin

Sub-Basin	Aspect	Max Soil Storage (mm)	Initial Soil Storage (%)	Max Infiltration Rate (mm/hr)	Clark U.H. T_c (hr)	Clark U.H. R (hr)
1	South	85.9	6.0	64.9	12.0	10.0
1	North	91.5	5.6	68.1	12.0	9.9
2	South	76.8	6.7	44.3	9.3	6.9
2	North	96.5	5.5	51.5	9.5	5.9
3	South	260.9	2.1	56.2	2.3	6.8
3	North	281.1	1.9	53.3	6.7	16.5

Table 3.10 Model parameters for Cheyenne Creek that are constant for all sub-basins

Aspect	Max Canopy Storage (mm)	Max Soil Percolation (mm/hr)	GW 1 Max Storage (mm)	GW 1 Storage Coefficient (hr)	L.R. GW 1. Storage Coefficient (hr)
South	1.5	82.9	0.04	29.8	29.8
North	7.2	82.9	0.04	29.8	29.8

Table 3.11 Calibration factors applied uniformly across all sub-basins for parameters estimated from physical properties and calibrated values for GW 1 parameters

Basin	Calibration factors				Calibrated parameters			
	Max Soil Storage (mm)	Max Infiltration Rate (mm/hr)	Clark Storage Coefficient R (hr)	Clark Time of Concentration T_c (hr)	GW 1 Max Storage (mm)	GW 1 Storage Coefficient (hr)	L.R. GW 1 Storage Coefficient (hr)	GW 1 Max Percolation (mm/hr)
Bear Creek	0.17	-	-	-	0.3	1	100	South: 0.5, North: 1.5
Big Thompson River	0.5	-	1.9	1.9	2	6	15	South: 0.5, North: 1.5
South Boulder Creek	0.7	-	3.0	-	2	3	60	South: 0.5, North: 2.0
Cheyenne Creek	0.6	-	3.5	3.5	5	3	40	South: 2.5, North: 3.5
N.F. Big Thompson River	0.8	1.3	1.2	0.1	4	8	8	South: 1.0, North: 3.0
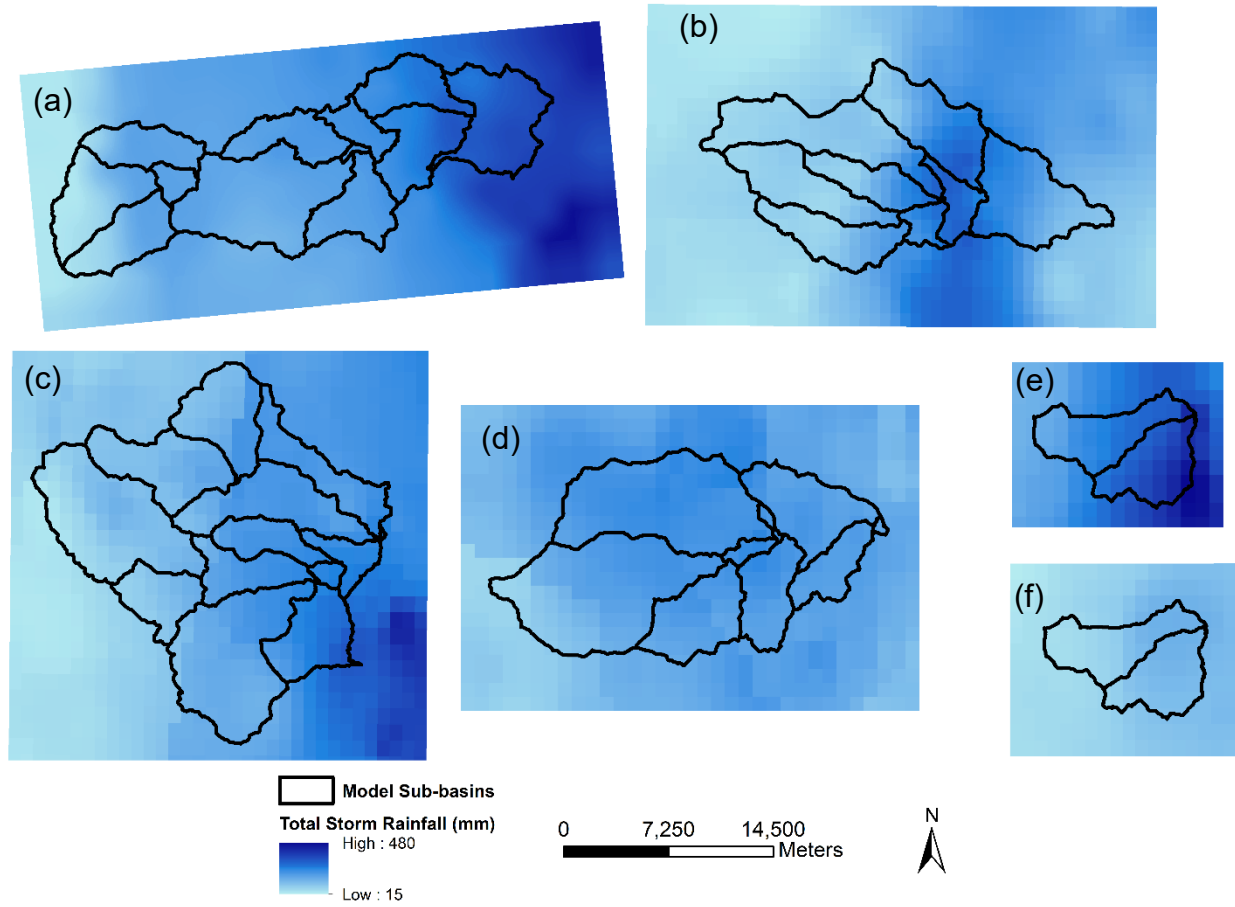
Figure 3.1 Total storm rainfall depth grids for (a) South Boulder Creek 2013 storm, (b) North Fork Big Thompson River 1976 Storm, (c) Big Thompson River 2013 Storm, (d) Bear Creek 2013 storm, (e) Cheyenne Creek 2013 storm, and (f) Cheyenne Creek 1997 storm with sub-basin boundaries
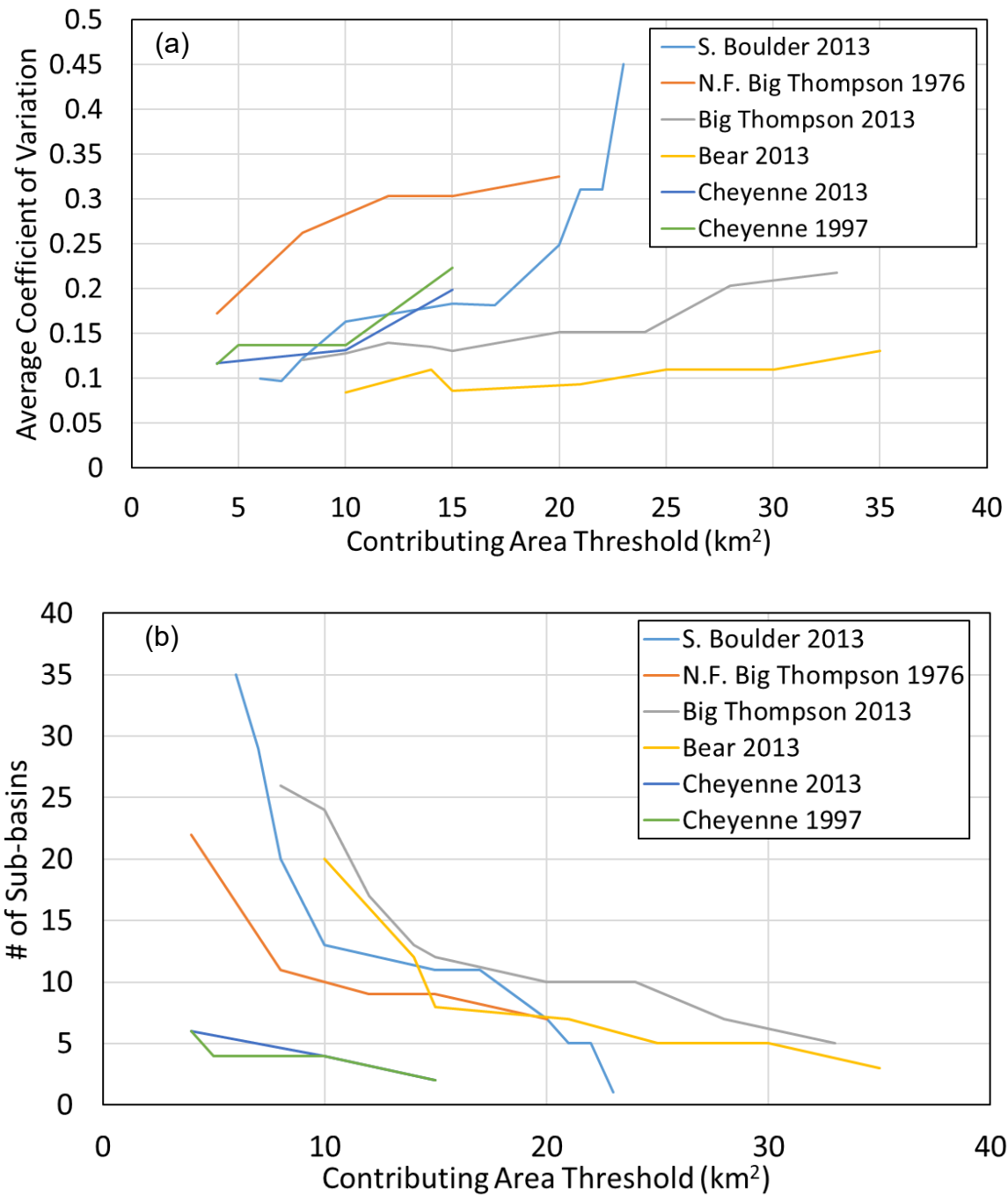
Figure 3.2 (a) Coefficient of variation of total storm depth averaged among sub-basins as a function of the contributing area threshold and (b) number of sub-basins as a function of the contributing area threshold
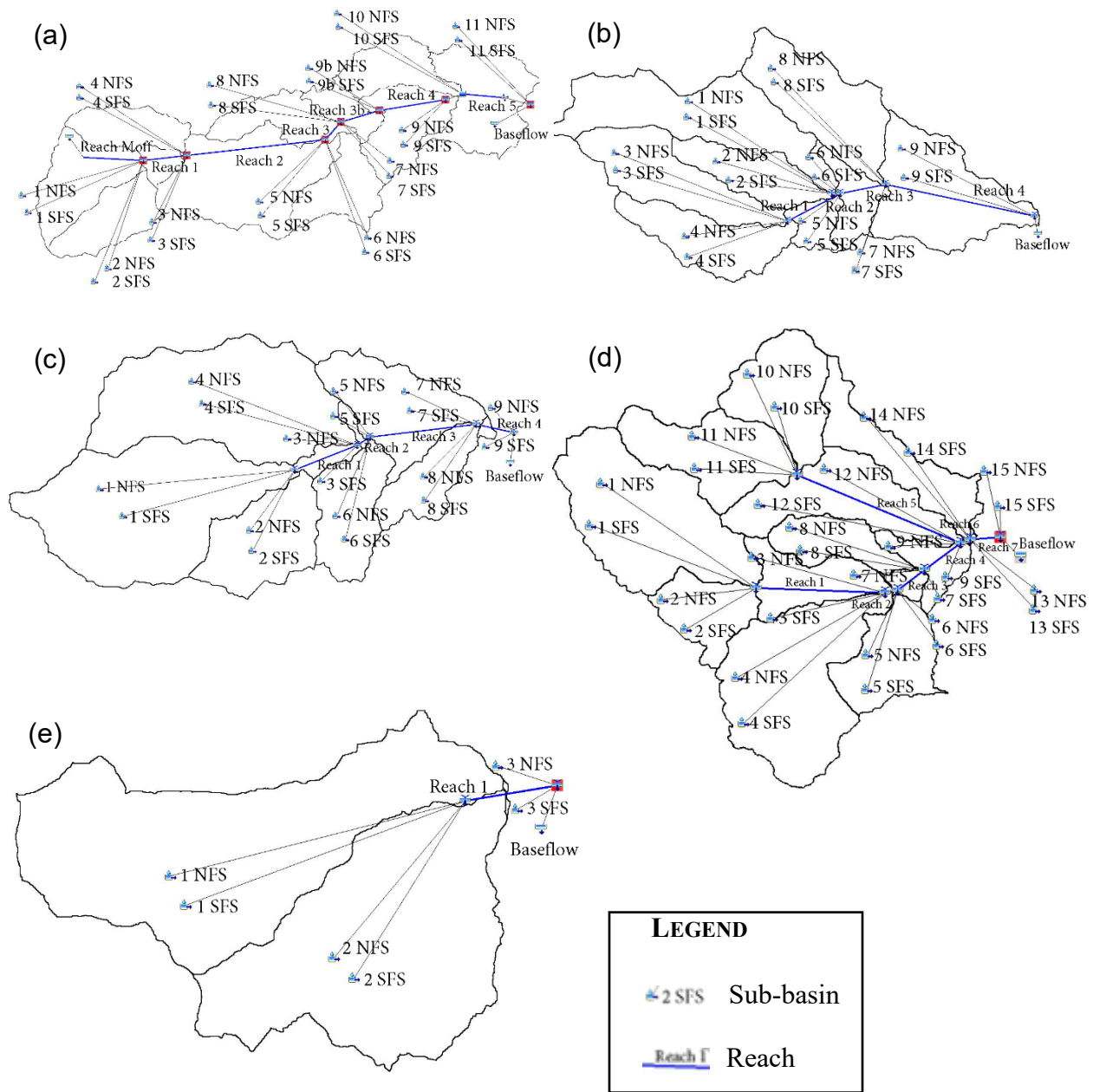
Figure 3.3 HEC-HMS model configurations for (a) South Boulder Creek, (b) North Fork Big Thompson River, (c) Bear Creek, (d) Big Thompson River, and (e) Cheyenne Creek
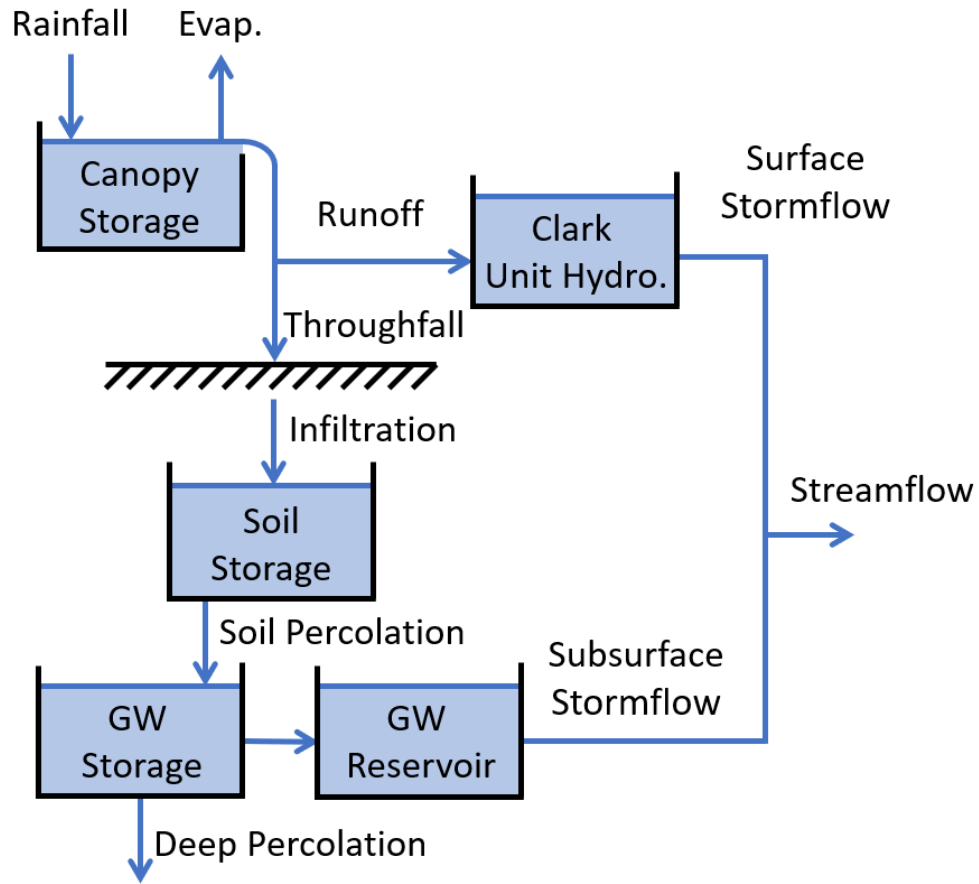
Figure 3.4 Water storage and pathways in the HEC-HMS models
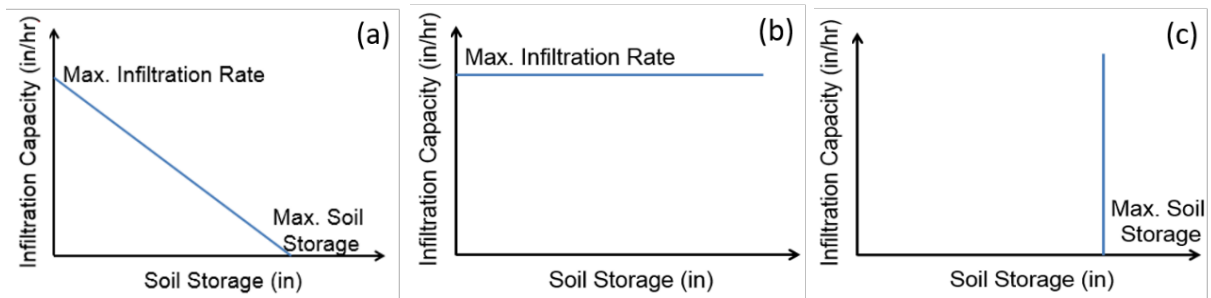
Figure 3.5 Infiltration capacity as a function of soil storage (a) for typical conditions, (b) when maximum soil storage is very large, and (c) when maximum infiltration rate is very large

4. RESULTS

4.1 Historical Storms

4.1.1 September 2013 South Boulder Creek

The observed rainfall intensity, observed streamflow, and modeled streamflow for the 2013 storm in SBC are shown in Figure 4.1. The observed streamflow exhibits two peaks, and the second peak is higher than the first one despite the rainfall intensity being lower later in the storm. The modeled streamflow also exhibits two peaks with the second one being higher, but the second peak is underestimated. The modeled hydrograph recessions exhibit similar behavior to the observations, but the model misses the small peak that occurs toward the end of the storm period. Nearly all the modeled streamflow is produced by Sub-Basin 11 NFS and Sub-Basin 11 SFS, which are the only sub-basins downstream of Gross Reservoir. This behavior is consistent with observations, which indicate Gross Reservoir retained nearly all the flow from upstream. Surface runoff from Sub-Basin 11 produces the peak flows for both NFS and SFS, while subsurface stormflow contributes nearly all the discharge during periods with lower flows. Sub-Basin 11 SFS produces substantially more surface runoff than Sub-Basin 11 NFS.

The degree of saturation for the soil layer in Sub-basin 11 NFS and SFS is shown in Figure 4.2. Both NFS and SFS exceed 85% saturation when surface runoff is produced, indicating saturation-excess is the dominant runoff mechanism. The SFS saturate for a longer period during the storm than the NFS, which is consistent with the greater runoff volume from the SFS.

A model simulation was run that prohibits saturation-excess runoff and forces infiltration-excess runoff. The soil storage capacity was increased to a very large value, and the maximum infiltration capacity was calibrated to reproduce the observed hydrograph as closely as possible. This approach requires the infiltration capacity to be calibrated to half of the original parameterization. In addition, the modeled hydrograph matches the first peak in the observed hydrograph, but the second peak is absent, and the rest of the hydrograph is inaccurate (not shown). These results also suggest saturation-excess was the dominant mechanism during the 2013 storm.

Soil moisture observations were also obtained from the National Science Foundation's Boulder Creek Critical Zone Observatory (CZO) for the 2013 storm (Anderson et al. 2019). The CZO consisted of three monitoring sites—Betasso, Lower Gordon Gulch, and Upper Gordon Gulch—with instrumentation at multiple locations in each site. In total, six sensors were on SFS, four were on NFS, and one was in a flat valley bottom. Sensor depths ranged from 50 to 1,380 mm. Figure 4.3a shows the soil moisture (volumetric water content) at the flat location (site P5). The soil moisture at each depth reached a high constant value, which is inferred as the saturation point. Saturation occurred first at the deepest sensor and last at the shallowest sensor. Figure 4.3b shows the site P6 data, which are typical for SFS. Saturation is inferred at the 250-mm depth because a plateau is seen. Saturation also likely occurred briefly at the 50-mm depth due to the very high soil moisture values (above 0.5). Again, saturation occurred first at the 250-mm depth and last at the 50-mm depth. This behavior is consistent with saturation-excess runoff where saturation begins on the low-permeability layer and progresses upwards until reaching the ground surface (at which point runoff is produced). It is inconsistent with infiltration-excess runoff, which produces saturation first at the top of the soil column. Site P4, which is typical of an NFS, did not reach saturation (Figure 4.3c). Throughout the CZO, probable saturation occurred at approximately 40% of the monitoring locations on SFS and 0% of the locations on NFS. The aspect-dependent saturation is consistent with the more frequent debris flow occurrence on SFS than NFS (Ebel et al. 2015; McGuire et al. 2016; Rengers et al. 2016; Timilsina 2019).

4.1.2 July-August 1976 North Fork Big Thompson River

The observed rainfall intensity, observed streamflow, and modeled streamflow for the 1976 storm in NFBTR are shown in Figure 4.4. The model produces a peak flow that is very similar to the observations, but the modeled peak occurs later than the observed peak. The observed peak streamflow occurs approximately one hour after the peak rainfall intensity, while the modeled peak streamflow occurs approximately two hours after the peak rainfall. Aside from the time delay, the model reproduces the shape of the observed hydrograph well.

The degree of saturation for the soil layer in Sub-Basin 3 NFS and Sub-Basin 3 SFS is provided in Figure 4.5. Sub-Basin 3 is shown because it produces the highest surface runoff volume of all the sub-basins in NFBTR. For both the NFS and SFS, the soil layer never exceeds 68% saturation, even when surface runoff is produced. This behavior indicates infiltration-excess is the dominant runoff mechanism because runoff occurs while much of the soil column remains unsaturated.

4.1.3 September 2013 Bear Creek

Figure 4.6 shows the rainfall intensity, observed streamflow, and modeled streamflow for Bear Creek for the 2013 storm. The model reproduces the timing and relative magnitude of the observed streamflow peaks as well as the slope of the observed recession limbs. However, the model shows a larger response to the early rainfall than the streamflow observations. Attempts were made to reduce the initial response in the model by increasing the basin's maximum soil storage and delaying the subsurface flow by increasing the GW 1 storage coefficient, but the remainder of the hydrograph was compromised, and a less accurate model resulted. The model also overpredicts the flow immediately after largest peak.

The saturation fraction for the soil layer in Sub-Basin 4 of the Bear Creek model is provided in Figure 4.7. Sub-Basin 4 is shown because it produces the highest peak flow for the 2013 storm. Sub-Basin 4 SFS briefly reaches saturation, but very little excess rainfall is produced during the storm. Subsurface stormflow is the dominant streamflow production mechanism for this case.

4.1.4 September 2013 Big Thompson River

Figure 4.8 shows the rainfall intensity, observed streamflow, and modeled streamflow for the Big Thompson River during the 2013 storm. The model reproduces the timing and magnitude of the observed peak streamflow. The model's streamflow recedes slightly slower than the observed streamflow, and the width of model's hydrograph peak is narrower than that of the observed hydrograph.

The saturation fraction for the soil layer in Sub-Basin 10, which produces the highest peak flow and the most surface runoff of all the sub-basins, is shown in Figure 4.9. The basin exceeds 85% saturation when excess rainfall is generated, indicating saturation-excess is the dominant runoff mechanism during the storm.

4.1.5 September 2013 Cheyenne Creek

The observed rainfall, observed streamflow, and modeled streamflow for Cheyenne Creek during the 2013 storm are shown in Figure 4.10. The model approximates the general behavior of the observed hydrograph, but it fails to capture the fine-scale variations in the observations. While the modeled hydrograph shows similar increasing and decreasing trends as the observed hydrograph, it frequently over- or under-estimates the actual streamflow.

Figure 4.11 shows the soil's degree of saturation for Sub-Basin 2 NFS and Sub-Basin 2 SFS because they are the only sub-basins that produce surface runoff. The soil layer exceeds 85% saturation when runoff is produced, suggesting saturation-excess runoff is the dominant mechanism.

4.1.6 June 1997 Cheyenne Creek

The observed rainfall, observed streamflow, and modeled streamflow for the 1997 storm in Cheyenne Creek are provided in Figure 4.12. The rainfall intensities never exceed 15 mm/hr during the storm, and the total rainfall depth is less 120 mm. The model produces similar timing of the observed streamflow peak, but it underestimates the magnitude of the peak.

The modeled saturation fraction for 2 NFS and Sub-Basin 2 SFS during the 1997 storm is shown in Figure 4.13 because they produce the most streamflow. The soil never approaches saturation, and the rainfall rate is never high enough to produce infiltration-excess runoff. Thus, no runoff occurs during the storm, and the modeled hydrograph is entirely subsurface stormflow.

4.1.7 Results Summary

Table 4.1 summarizes the model performance for all basins and storms. The root mean square error (RMSE), mean bias error (MBE), Nash-Sutcliffe coefficient of efficiency (NSCE) (Nash and Sutcliffe 1970), RMSE-observations standard deviation ratio (RSR) (Moriasi et al. 2007), and peak flow error are used to quantify model performance. Note that the observed hydrograph for NFBTR is incomplete so its performance metrics only consider the period with observations.

RMSE directly characterizes the model errors and has the same units as the streamflow. An RMSE of zero indicates perfect model performance, and increasing RMSE values indicate larger model errors. In general, the models of smaller basins (e.g., Cheyenne Creek) have lower RMSE values than models of larger basins (e.g., Big Thompson River). Both the observed and modeled streamflow values are smaller for small basins, so the RMSE values also tend to be smaller. The RMSE for NFBTR is substantially larger than the other basins even though it is one of the smaller study basins. The large RMSE occurs due to the high flows produced by the 1976 storm.

MBE indicates whether the model over- or under-predicts the observations on average. An MBE of zero indicates the model has no bias. A positive MBE suggests the model tends to overpredict, while a negative MBE suggests it typically underpredicts. Most of the models have positive MBE values, while the 1997 Cheyenne Creek and the NFBTR models have negative MBE values. The MBE values for the Big Thompson River, SBC, and 1997 Cheyenne Creek models are 2.5%, 8.4%, and 8.7%, respectively, of their respective average observed flows, indicating relatively good agreement. In contrast, the MBE values for the Bear Creek, 2013 Cheyenne Creek, and NFTBR models are 24.2%, 26.9%, and 17.7%, respectively, of their average observed flows, indicating poorer performance.

NSCE measures the model errors relative to the variability of the observations. An NSCE of 1 indicates the model perfectly matches the observations. RSR is the ratio of the RMSE and the standard deviation of the observed data. Lower RSR values indicate better model performance. Moriasi et al. (2007) developed performance ratings based on a review of numerous studies, which primarily analyzed long-term streamflow models with daily or monthly time steps. They proposed ratings of "Satisfactory" if $0.50 < NSCE \leq 0.65$ and $0.60 < RSR \leq 0.70$, "Good" if $0.65 < NSCE \leq 0.75$ and $0.50 < RSR \leq 0.60$, and "Very good" if $0.75 < NSCE \leq 1.00$ and $0.00 < NSCE \leq 0.50$. All the models developed in this study besides NFBTR have NSCE values of $0.69 - 0.90$ and RSR values of $0.32 - 0.56$, so they exceed the limit to be considered "Good." Half of the models have an NSCE greater than 0.75 and an

RSR less than 0.50, so they would be classified as "Very good." The basins that do not obtain a "Very good" classification are Cheyenne Creek (2013 and 1997 storms) and NFBTR. The Cheyenne Creek models were calibrated to have consistent parameters for both the 1997 and 2013 storm events. When calibrated separately, the model's NSCE values are 0.76 for the 2013 storm and 0.88 for the 1997 storm. Only a single storm was simulated for the other basins, so their performance may also deteriorate if multiple storms were considered. The NFBTR model performance misses the timing of the observed hydrograph peak, and the observed hydrograph is also incomplete, which exaggerates the importance of the peak in the NSCE and RSR calculations. If the timing of the peak flow were accurate, the model's scores would improve substantially.

The peak flow error is the difference between the observed and modeled peak flows. A positive value indicates that the model overpredicts the peak. Although the SBC model performs well according to the other metrics (which consider the overall hydrograph shape), it has the largest peak flow error magnitude because it substantially underestimates the second peak of the observed hydrograph (Figure 4.1). The NFBTR model has a relatively low peak flow error magnitude (despite having poorer performance by the other measures), and the Big Thompson River model has the lowest peak flow error magnitude among all the basins.

4.2   Design Storms

The saturation fraction for the two-hour, six-hour, and 72-hour PMP storms for SBC and NFBTR are shown in Figure 4.14. For the two-hour storms in both basins (Figure 4.14a and 4.14b), the soil does not approach saturation when runoff occurs, which indicates infiltration-excess runoff is the dominant mechanism. For the six-hour design storms, the soil exceeds 85% saturation when runoff occurs in SBC, which indicates saturation-excess runoff dominates (Figure 4.14c). In the NFBTR basin, the saturation fraction differs by sub-basin for the six-hour storm (Figure 4.14d). In some sub-basins the saturation fraction exceeds 85%, indicating saturation-excess runoff is likely. Other sub-basins have lower saturation fractions, which suggests infiltration-excess runoff or perhaps a combination of runoff types occurs. For the 72-hour PMP, the soil exceeds 85% saturation in both basins, which indicates saturation-excess runoff is the dominant runoff mechanism (Figure 4.14e and 4.14f). Figure 4.14 shows the saturation fraction increases and decreases linearly for large durations of all PMP storms in each basin. This behavior occurs because the linear function for soil storage approximates a linear reservoir and does not contain the exponential decay term characteristic of a typical linear reservoir. Therefore, when infiltration into the soil storage is constant, saturation fraction exhibits a linear trend.

Table 4.2 summarizes the model results for all basins for the PMP and the AEP design storms. The controlling storm column indicates the storm duration that produces the highest peak streamflow and thus would dictate the design for the given AEP or PMP. The runoff mechanism column indicates whether the infiltration-excess or saturation-excess mechanism produces the runoff for the controlling storm. When a single mechanism exists, infiltration-excess runoff occurs for all two-hour storms that are the controlling event, and saturation-excess runoff occurs for all six-hour and 48-hour storms that are the controlling event (except one case where no surface runoff occurs). Longer storms typically have lower rainfall intensities but larger total depths that saturate the soil. For example, the 72-hour PMP in SBC has a total rainfall depth of 422 mm, while the two-hour PMP has a depth of only 117 mm. Shorter storms exhibit higher rainfall intensities that can exceed infiltration capacities. The two-hour PMP in SBC has a peak rainfall intensity of 157 mm/hr, while the 72-hour PMP has a peak intensity of only 30.5 mm/hr.

Table 4.1 Storm duration and model performance metrics for all basins and events

Basin	Storm	Rainfall Duration (hr)	RMSE (m³/s)	MBE (m³/s)	NSCE	RSR	Peak Flow Error (m³/s)	Runoff Mechanism
Bear Creek	2013	180	4.90	3.72	0.83	0.42	-2.8	None
Big Thompson River	2013	172	7.34	0.56	0.89	0.32	-0.6	Saturation-Excess
Cheyenne Creek	2013	144	4.40	1.41	0.68	0.56	-8.5	Saturation-Excess
South Boulder Creek	2013	154	4.31	0.65	0.83	0.41	-22.7	Saturation-Excess
Cheyenne Creek	1997	34	1.74	-0.41	0.71	0.54	-6.4	None
N.F. Big Thompson River	1976	50	64.0	-23.43	0.48	0.71	3.5	Infiltration-Excess

Table 4.2 Controlling storm duration and dominant runoff mechanism for probable maximum precipitation (PMP) and annual exceedance probability (AEP) design storms using models calibrated to the historical storms.

Basin	Storm Type	Controlling Storm Duration	Peak Rainfall Intensity (mm/hr)	Total Storm Depth (mm)	Runoff Mechanism
Bear Creek	PMP	6 hr	47.5	158	Saturation-Excess
	10^{-7} AEP	6 hr	45.6	143	Saturation-Excess
	10^{-6} AEP	6 hr	38.5	120	Saturation-Excess
	10^{-5} AEP	2 hr	133.4	73	Both
	10^{-4} AEP	6 hr	25.7	80	Saturation-Excess
	10^{-3} AEP	48 hr	12.6	139	Saturation-Excess
Big Thompson River	PMP	72 hr	22.3	339	Saturation-Excess
	10^{-7} AEP	48 hr	26.9	297	Saturation-Excess
	10^{-6} AEP	48 hr	22.7	2501	Saturation-Excess
	10^{-5} AEP	48 hr	18.7	207	Saturation-Excess
	10^{-4} AEP	2 hr	87.8	48	Infiltration-Excess
	10^{-3} AEP	2 hr	68.0	37	Infiltration-Excess
Cheyenne Creek	PMP	2 hr	327.4	249	Infiltration-Excess
	10^{-7} AEP	48 hr	41.4	458	Saturation-Excess
	10^{-6} AEP	48 hr	34.3	379	Saturation-Excess
	10^{-5} AEP	48 hr	27.8	308	Saturation-Excess
	10^{-4} AEP	2 hr	151.1	83	Infiltration-Excess
	10^{-3} AEP	2 hr	119.0	65	Infiltration-Excess
North Fork Big Thompson River	PMP	2 hr	222.8	169	Infiltration-Excess
	10^{-7} AEP	2 hr	191.6	105	Infiltration-Excess
	10^{-6} AEP	2 hr	160.6	88	Infiltration-Excess
	10^{-5} AEP	2 hr	132.0	76	Infiltration-Excess
	10^{-4} AEP	2 hr	105.5	58	Infiltration-Excess
	10^{-3} AEP	48 hr	12.4	137	None
South Boulder Creek	PMP	72 hr	30.48	422	Saturation-Excess
	10^{-7} AEP	48 hr	30.2	334	Saturation-Excess
	10^{-6} AEP	2 hr	160.8	88	Infiltration-Excess
	10^{-5} AEP	2 hr	133.2	80	Infiltration-Excess
	10^{-4} AEP	2 hr	107.6	59	Infiltration-Excess
	10^{-3} AEP	48 hr	12.6	132.2	Both

Figure 4.1 Observed rainfall intensity and comparison of observed and modeled streamflow at the BOCELSCO stream gauge (i.e., the outlet of the South Boulder Creek basin) for the 2013 storm

Figure 4.2 Degree of saturation for the 2013 storm in the South Boulder Creek model for (a) Sub-Basin 11 NFS and (b) Sub-Basin 11 SFS
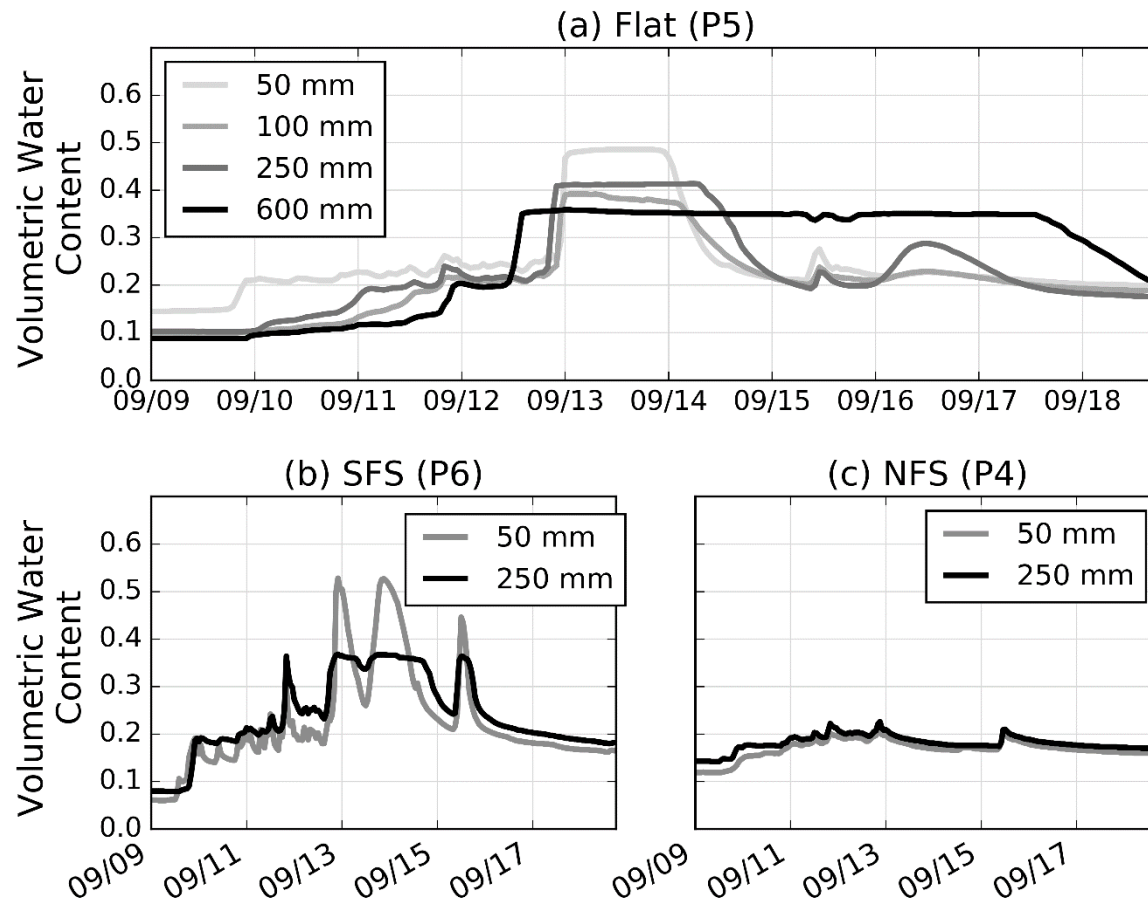
Figure 4.3 In-situ soil moisture observations from the Boulder Creek Critical Zone Observatory during the September 2013 flood on (a) a flat valley bottom, (b) SFS, and (c) NFS
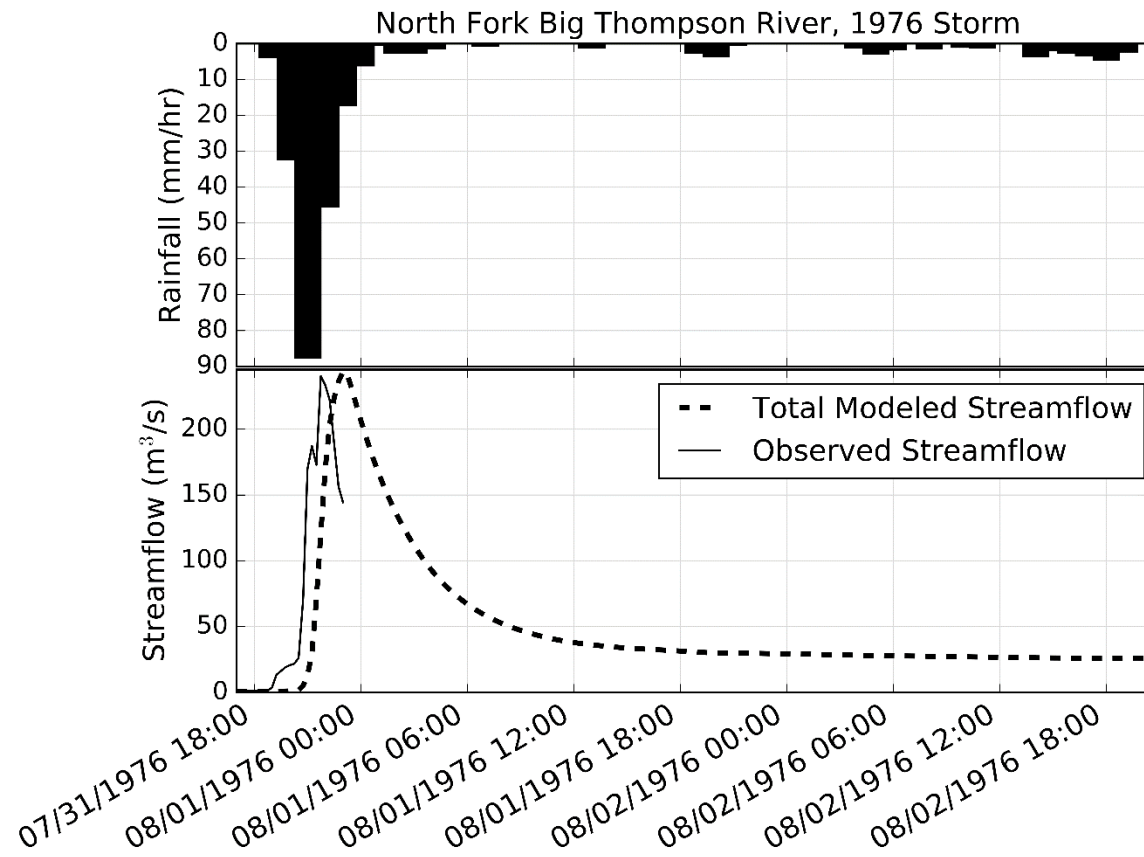
Figure 4.4 Observed rainfall intensity and comparison of observed and modeled streamflow at the BTNFDRCO stream gauge location (i.e., the outlet of the North Fork Big Thompson River basin) for the 1976 storm
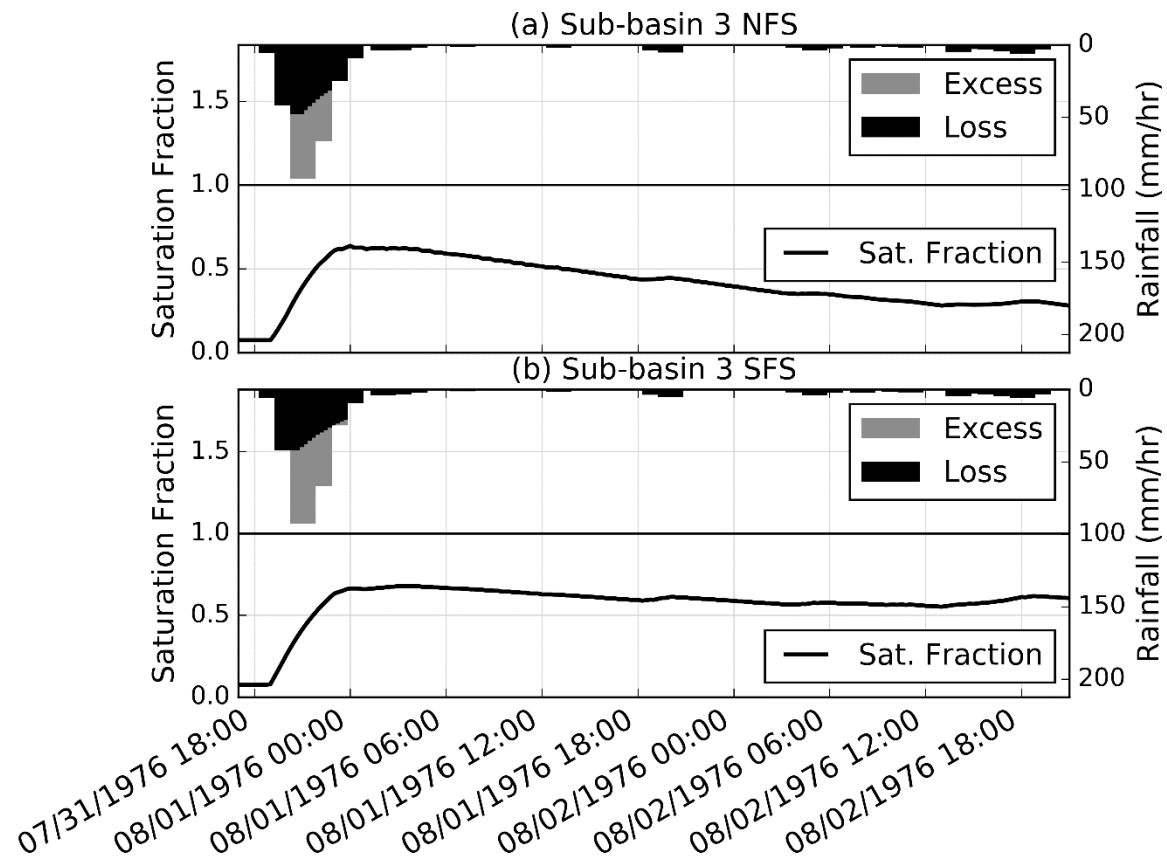
Figure 4.5 Degree of saturation for the 1976 storm in the North Fork Big Thompson River model for (a) Sub-Sasin 3 NFS and (b) Sub-Basin 3 SFS
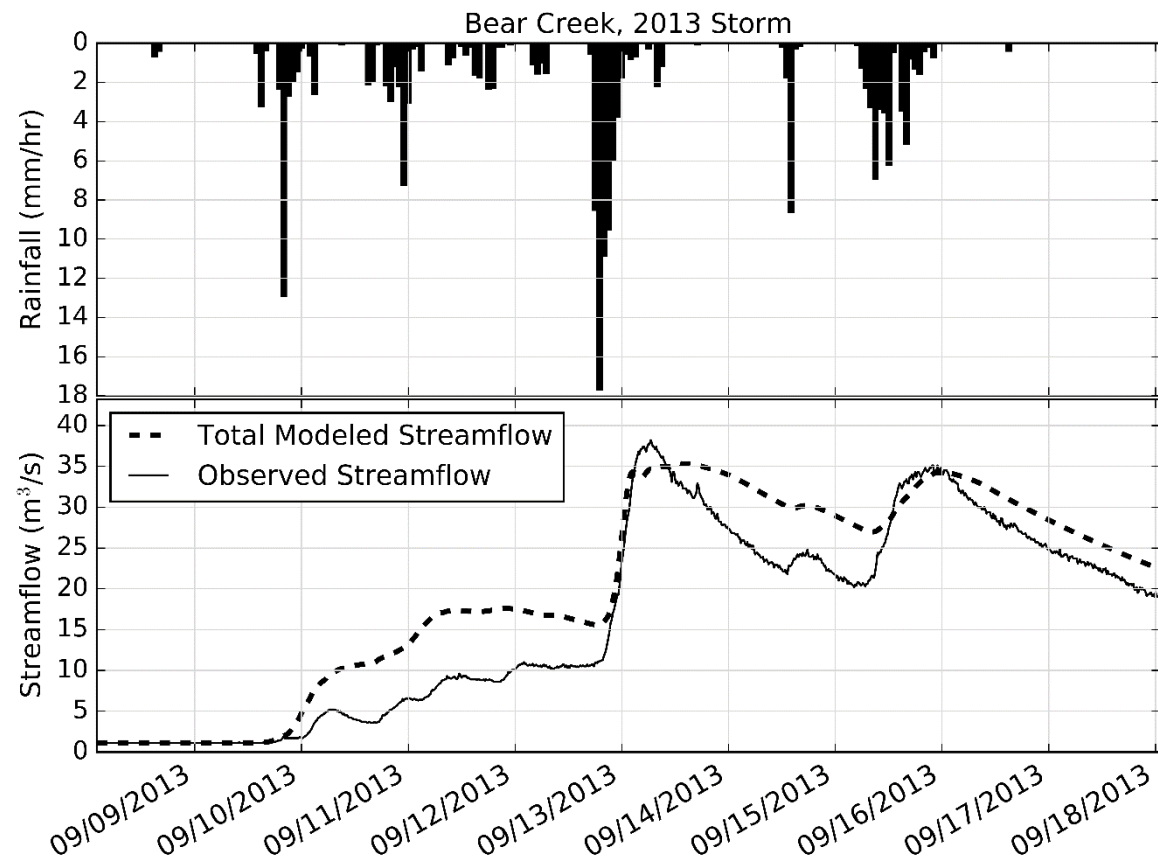
Figure 4.6 Observed rainfall intensity and comparison of observed and modeled streamflow at the BCREVRCO stream gauge (i.e., outlet of the Bear Creek basin) for the 2013 storm
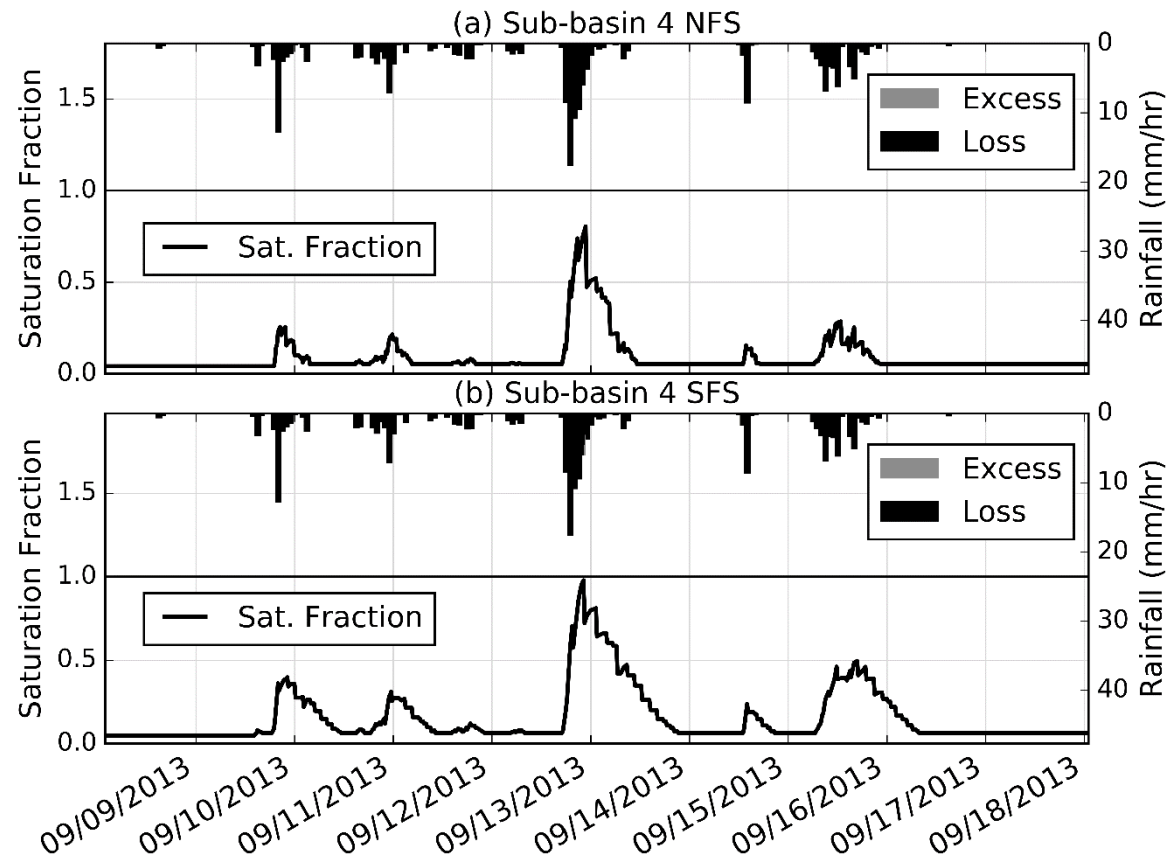
Figure 4.7 Degree of saturation for the 2013 storm in the Bear Creek model for (a) Sub-Basin 4 NFS and (b) Sub-Basin 4 SFS
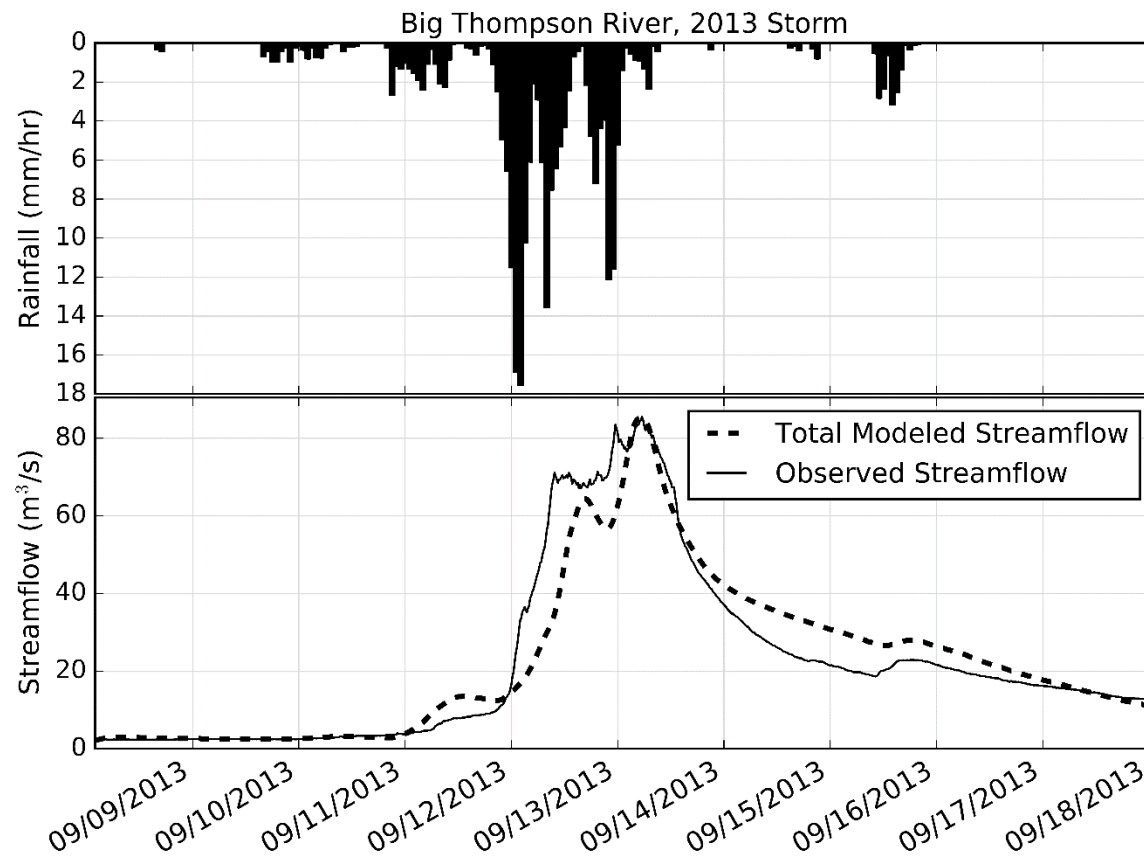
Figure 4.8 Observed rainfall intensity and comparison of observed and modeled streamflow at the BTABESCO stream gauge (i.e., outlet of the Big Thompson River basin) for the 2013 storm

35
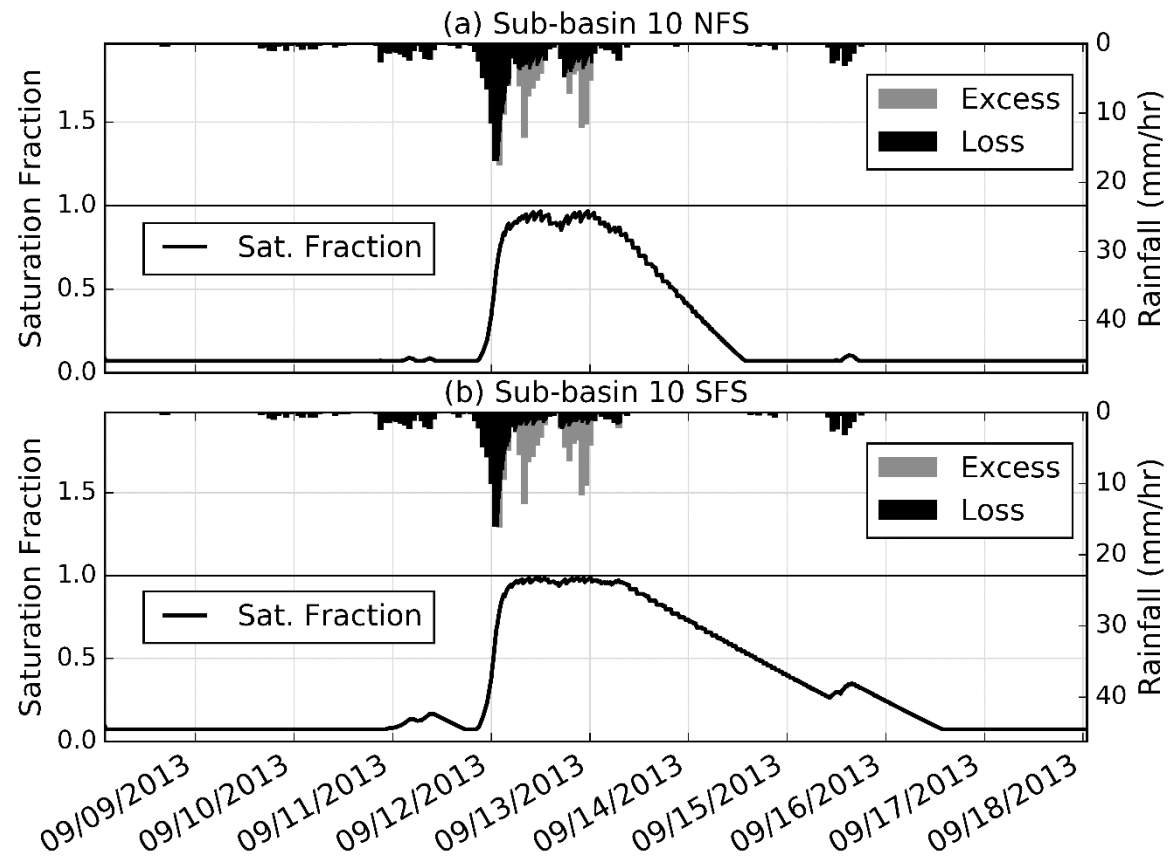
Figure 4.9 Degree of saturation for the 2013 storm in the Big Thompson River model for (a) Sub-Basin 10 NFS and (b) Sub-Basin 10 SFS
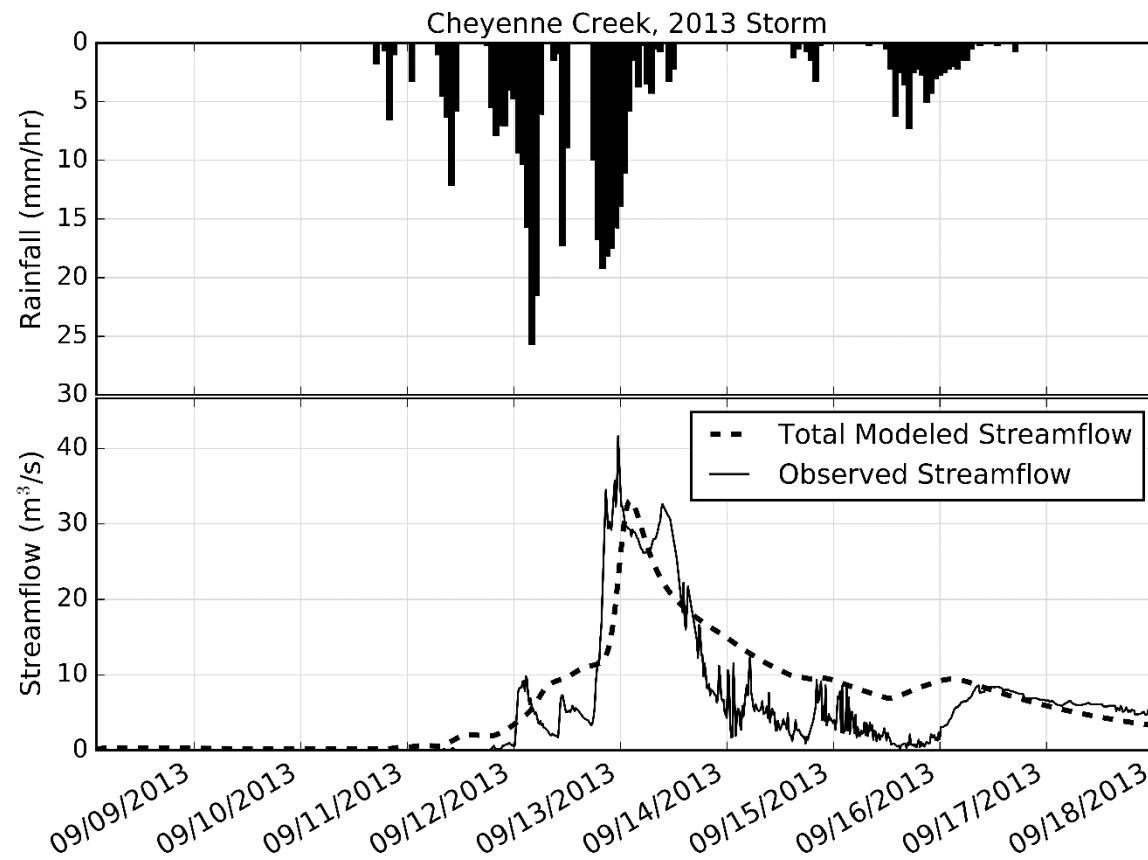
Figure 4.10 Observed rainfall intensity and comparison of observed and modeled streamflow at the CHEEVACO stream gauge (i.e. outlet of the Cheyenne Creek basin) for the 2013 storm
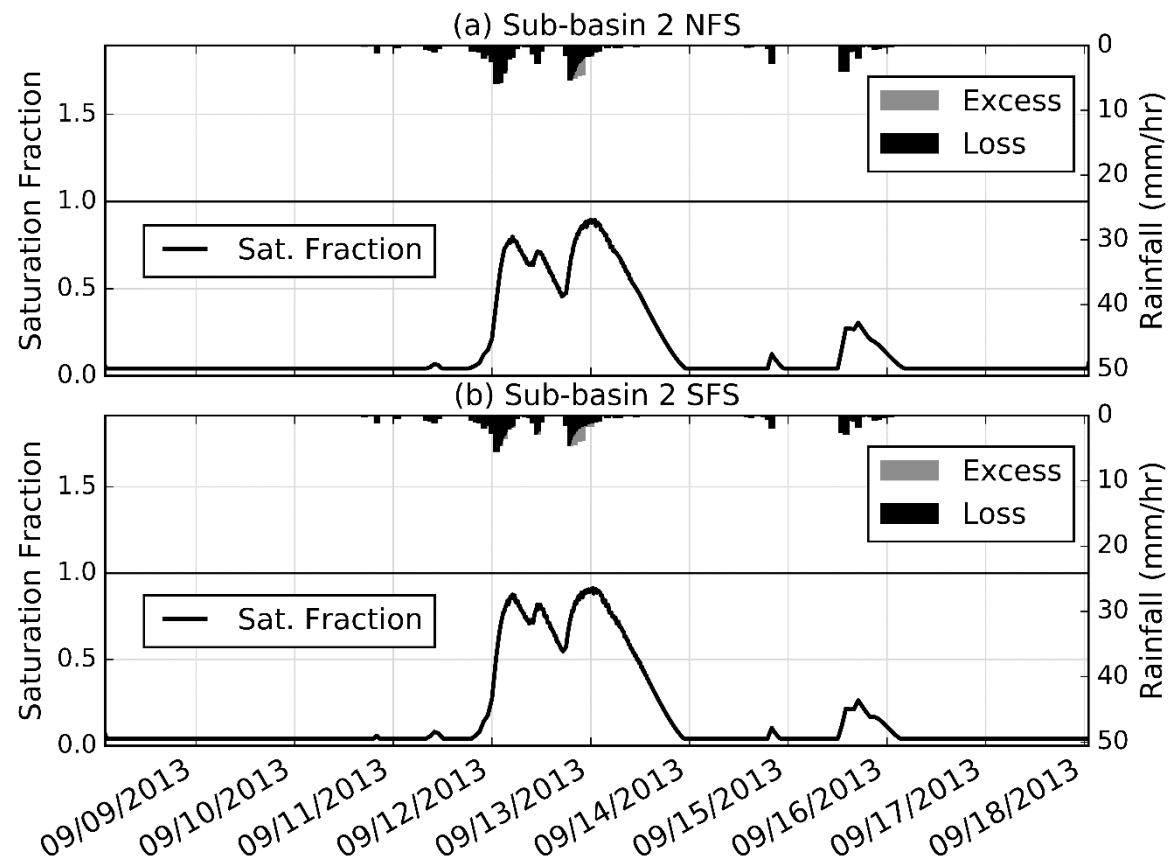
Figure 4.11 Degree of saturation for the 2013 storm in the Cheyenne Creek model for (a) Sub-Basin 3 NFS and (b) Sub-Basin 3 SFS
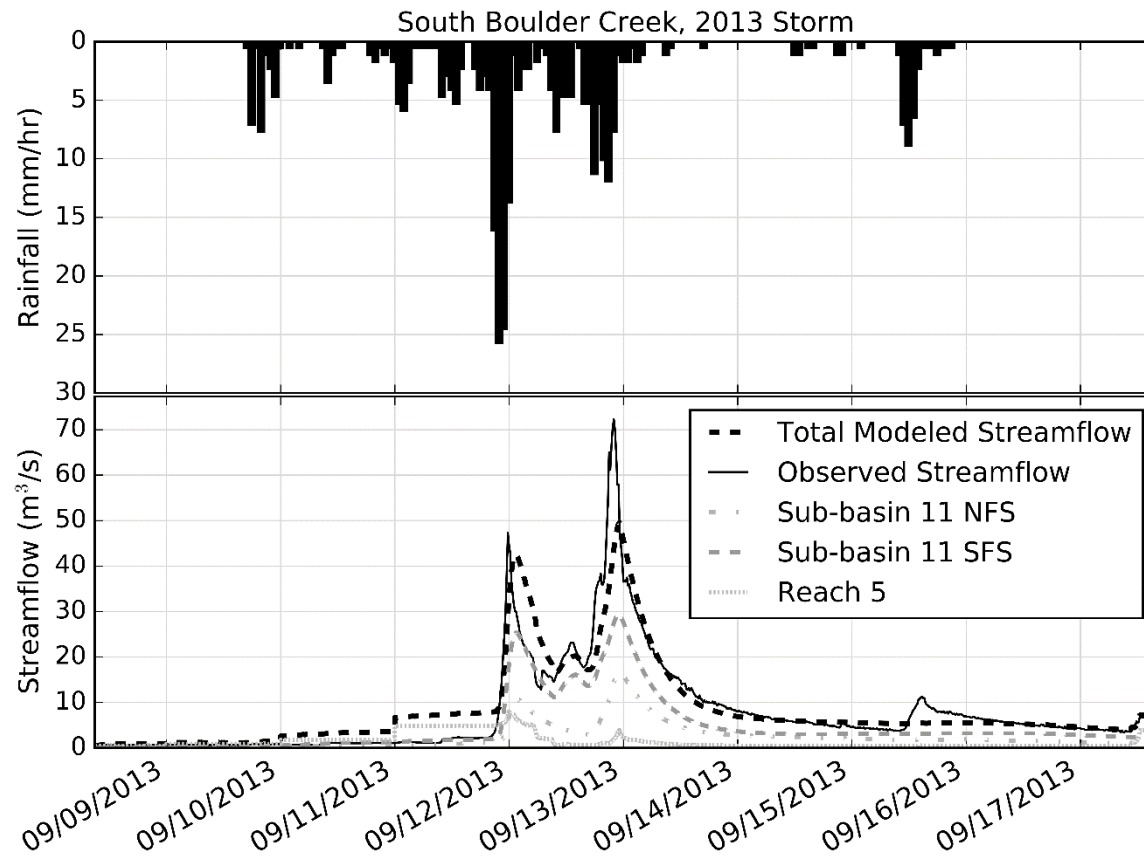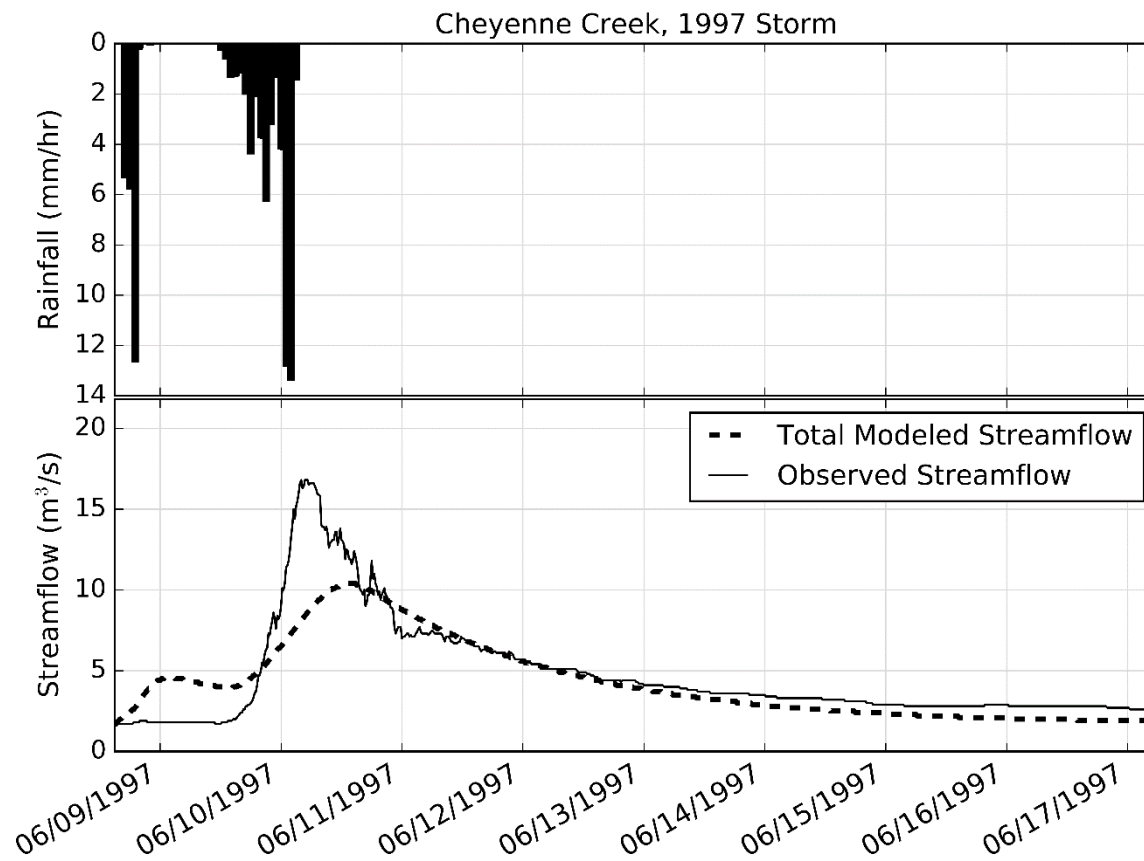
Figure 4.12 Observed rainfall intensity and comparison of observed and modeled streamflow at the CHEEVACO stream gauge (i.e., outlet of the Cheyenne Creek basin) for the 1997 storm
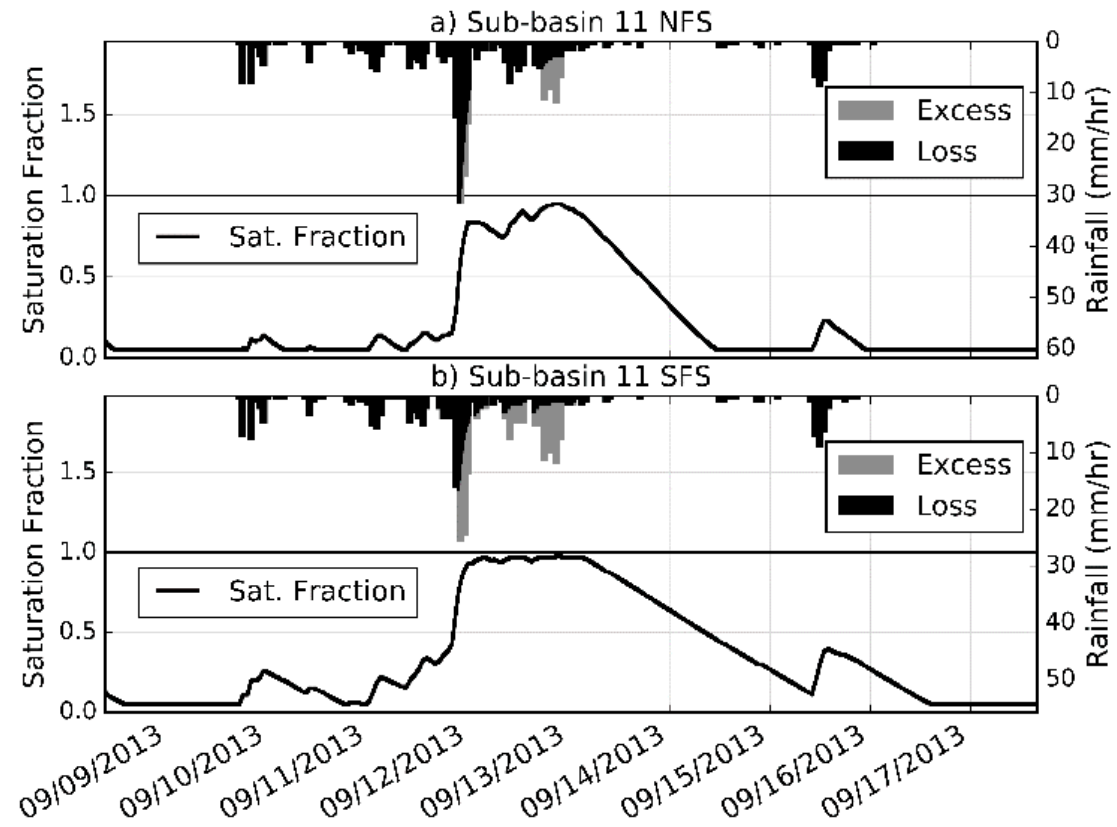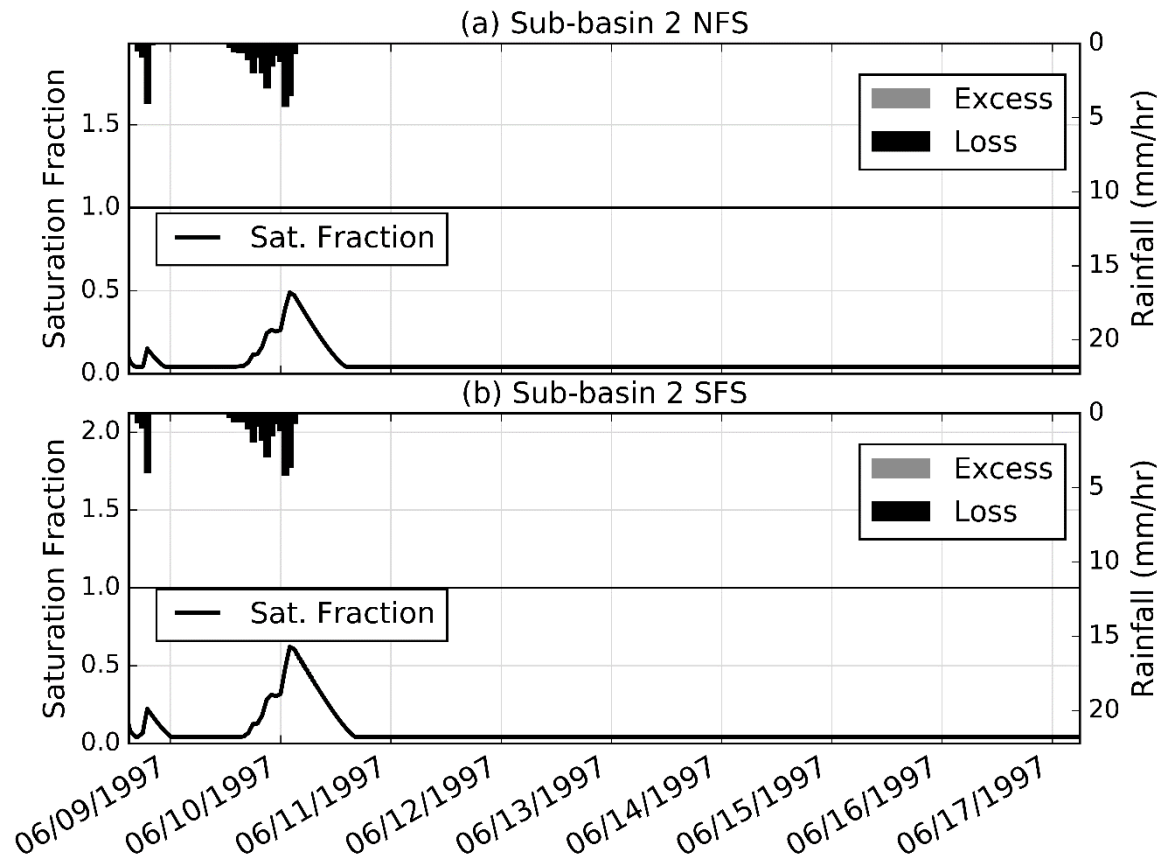
Figure 4.13 Degree of saturation for the 1997 storm in the Cheyenne Creek model for (a) Sub-Basin 1 NFS and (b) Sub-Basin 1 SFS
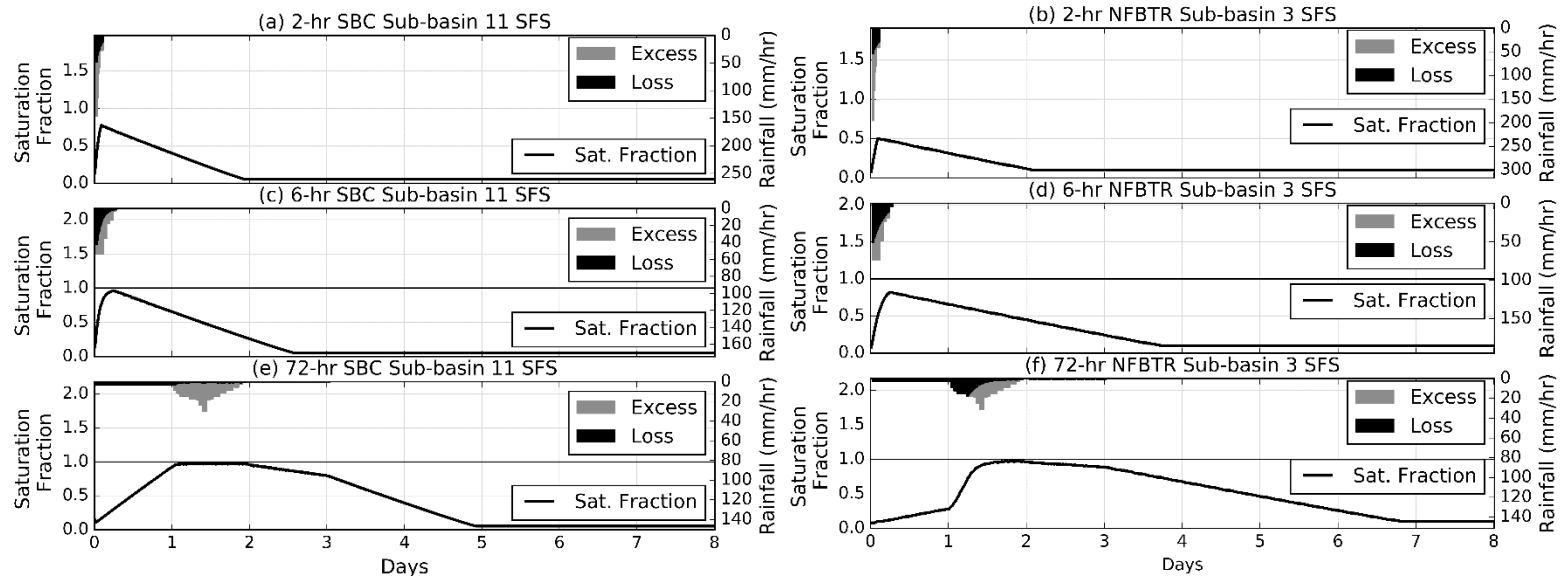
Figure 4.14 Degree of saturation for Sub-Basin 11 SFS in the South Boulder Creek (SBC) model for the (a) 2-hr Probable Maximum Precipitation (PMP), (c) 6-hr PMP, and (e) 72-hr PMP, and the degree of saturation for Sub-Basin 3 SFS in the North Fork Big Thompson River (NFBTR) model for the (b) 2-hr PMP, (d) 6-hr PMP, and (f) 72-hr PMP

4. CONCLUSIONS

This study aimed to determine the streamflow production mechanisms that were active for large historical storms in the Colorado Front Range and would be active for design storms used for hydrologic design evaluations and to propose modeling methods that can be used to simulate these mechanisms. Hydrologic models were developed using SMA in HEC-HMS. Historical storms from 1976, 1997, and 2013 as well as PMP and AEP design storms of various durations were simulated for five basins. The following conclusions can be drawn from this study:

- SMA in HEC-HMS can be used to simulate both saturation-excess and infiltration-excess runoff production. SMA calculates the soil's infiltration capacity as a function of the water stored in the soil and includes a maximum allowable storage. In the extreme case where the maximum soil storage is very large, this infiltration capacity function returns to the constant value that is assumed in some existing dam safety guidelines and describes infiltration-excess runoff. For the other extreme case where the maximum infiltration capacity is very large, unlimited infiltration occurs until the soil is completely saturated, which corresponds to saturation-excess runoff production. For the intermediate case, both mechanisms can occur. When this model was applied to the historical storms, it was able to reproduce the observed hydrographs with good to very good accuracy according to the standards proposed by Moriasi et al. (2007) for five of six model simulations.

- Saturation-excess runoff was the dominant runoff production mechanism during the 2013 storm for all basins considered where runoff occurred. For all those basins, the soil layer in the HEC-HMS models approached saturation when runoff was being produced. Furthermore, for SBC, a model that was forced to rely on infiltration-excess runoff could not reproduce the double peak in the observed hydrograph. Also, in-situ soil moisture observations during the event show saturation occurred first at the bottom of the soil profile and progressed upwards. This behavior is consistent with saturation-excess runoff but not infiltration-excess runoff, which saturates from above. The 2013 storm was an MLC event and had low rainfall intensities, but it produced as much as 380 mm of rainfall over the eight-day storm duration. The low rainfall intensities but large rainfall depth led to the dominance of saturation-excess runoff.

- Infiltration-excess runoff was likely the dominant mechanism for the 1976 storm in the NFBTR basin. In this case, the soil layer in the HEC-HMS model did not approach complete saturation when runoff was being produced. Thus, runoff occurred because rainfall intensity exceeded the non-zero infiltration capacity of the soil. The 1976 storm was an MEC event. It had relatively high rainfall intensities, delivering most of its 300 mm of rainfall in a three-hour period, but its total depth was lower than the 2013 event.

- Surface runoff likely did not occur for the 1997 storm in Cheyenne Creek. In this case, the entire streamflow hydrograph was produced by subsurface stormflow. The storm had a low total rainfall depth (120 mm) and peak intensities (1.4 mm/hr) compared with the 1976 and 2013 storms.

- Both saturation-excess runoff and infiltration-excess runoff can occur for the controlling design storms between the 10^{-3} AEP and the PMP. For a given AEP, when the two-hour design storm produces the highest peak streamflow and thus would control the design, infiltration-excess runoff is the dominant mechanism for all the basins considered. When the six-hour design storm or longer controls, saturation-excess runoff is the dominant runoff production mechanism. This result and the results for the historical events suggest hydrologic guidelines in this region should include the possibility of both saturation-excess and infiltration-excess runoff production.

The modeling methods used in this study are expected to be applicable to hydrologic analyses in other mountain basins, but additional research is needed in several areas. First, the methods should be tested for basins in other mountain ranges in Colorado and other regions. Other basins may have different lithology and vegetation cover and may experience storms with different characteristics than the Front Range and thus may behave differently. Second, the modeling methods should be examined to explore

potential simplifications. For example, NFS and SFS were modeled separately in this study due to their observed differences in vegetation cover and soil properties, but combining the hillslopes might produce predictions with similar accuracy. Also, the time-area curve for each sub-basin was developed from the configuration of that sub-basin, but a representative time-area curve may be adequate. Third, the parameter estimation methods should be extended and improved so the model can be applied to ungauged basins. Most methods used in this study could be applied to ungauged basins, but appropriate methods need to be developed for the groundwater related parameters. Fourth, uncertainty in the model predictions should be quantified. It is important to determine the parameters that introduce the most uncertainty so data collection efforts can better constrain the values of those parameters. For example, canopy interception data are currently limited to the Cache la Poudre catchment. Obtaining additional data for large storms throughout the Front Range would provide better constraints on the canopy parameters in the model. Finally, the nonlinear response of basins to storm events needs to be considered. Time of concentration is expected to depend on the depth of flow. When the flow is deeper, a smaller portion of the water is exposed to the bed friction, so the velocities are higher. The higher velocities are expected to increase peak flows and might affect modeling results.

REFERENCES

Anderson, S. P., Anderson, R. S., Hinckley, E. L. S., Kelly, P., and Blum, A. (2011). "Exploring weathering and regolith transport controls on Critical Zone development with models and natural experiments." *Applied Geochemistry*, Elsevier Ltd, 26, S3–S5.

Anderson, S. P., Hinckley, E.-L., Kelly, P., and Langston, A. (2014). "Variation in Critical Zone Processes and Architecture across Slope Aspects." *Procedia Earth and Planetary Science*, Elsevier B.V., 10, 28–33.

Anderson, S. P., Hinckley, E.-L., Rock, N., and Ragar, D. (2019). "CZO Dataset: Gordon Gulch: Lower - Soil Temperature, Soil Moisture (2009-2019) - Soil Sensors (GGL)SPTran_SLTmpSLMist_Array)." *Boulder Creek Critical Zone Observatory*, <http://criticalzone.org/boulder/data/dataset/2426/> (Jun. 11, 2017).

Andréassian, V., Oddos, A., Michel, C., Anctil, F., Perrin, C., and Loumagne, C. (2004). "Impact of spatial aggregation of inputs and parameters on the efficiency of rainfall-runoff models: A theoretical study using chimera watersheds." *Water Resources Research*, 40(5), 1–9.

Applied Weather Associates. (2018). "Cheyenne Creek 1997 Storm Precipitation Analysis System."

Bouwer, H. (1964). "Unsaturated flow in ground-water hydraulics." *Journal of the Hydraulics Division, Proceedings of the American Society of Civil Engineering*, 90(HY5).

Boyle, D. P., Gupta, H. V, and Sorooshian, S. (2000). "Toward improved calibration of hydrologic models Combining the strengths of manual and automatic methods." *Water Resources Research*, 36(12), 3663–3674.

Brater, E. F. (1968). "Steps toward a better understanding of urban runoff processes." *Water Resources Research*, 4(2), 335–347.

Capesius, J. P., and Stephens, V. C. (2009). *Regional Regression Equations for Estimation of Natural Streamflow Statistics in Colroado Scientific Investigations Report 2009-5136*. Reston, VA.

Chow, V. Te. (1959). *Open-Channel Hydraulics*. (H. E. Davis, ed.), McGraw-Hill Book Company, Inc.

Chow, V. Te, Maidment, D. R., and Mays, L. W. (1988). *Applied Hydrology*. McGraw-Hill Book Company.

Clark, C. O. (1945). "Storage and the unit hydrograph." *American Society of Civil Engineers Transactions*, 2261, 1410–1446.

Coleman, M. L., and Niemann, J. D. (2013). "Controls on topographic dependence and temporal instability in catchment-scale soil moisture patterns." *Water Resources Research*, 49, 1625–1642.

Colorado Division of Water Resources, and New Mexico Office of the State Engineer. (2018). *Colorado-New Mexico Regional Extreme Precipitation Study*.

Comair, G. F., McKinney, D. C., and Siegel, D. (2012). "Hydrology of the Jordan River Basin: Watershed Delineation, Precipitation and Evapotranspiration." *Water Resources Management*, 26(14), 4281–4293.

Cudworth, A. G. (1989). *Flood Hydrology Manual: A Water Resources Technical Publication*.

Djokic, D., Ye, Z., and Dartiguenave, C. (2011). *Arc Hydro Tools Overview Version 2.0*.

Dunn, C., Hurst, M., Dotson, H., McPherson, M., Doan, J., and Evans, T. (2001). *HEC-HMS for the Sacramento and San Joaquin River Basins Comprehensive Study*. Sacramento, CA.

Dunne, T. (1978). "Field studies of hillslope flow processes." *Hillslope Hydrology*, ed. by M.J, 227–293.

Dunne, T., and Black, R. D. (1970a). "Partial Area Contributions to Storm Runoff in a Small New England Watershed." *Water Resources Research*, 6(5), 1296–1311.

Dunne, T., and Black, R. D. (1970b). "An Experimental Investigation of Runoff Production in Permeable Soils." *Water Resources Research*, 6(2), 478–490.

Eagleson, P. S. (1970). *Dynamic Hydrology*. McGraw-Hill Book Company, New York.

Ebel, B. A. (2013). "Wildfire impacts on soil-water retention in the Colorado Front Range, United States." *Water Resources Research*, 48(12), 1–12.

Ebel, B. A. (2016). *Soil depth and soil-hydraulic properties of Sugarloaf experimental catchment; 2010 Fourmile Canyon Fire area, Colorado*.

Ebel, B. A., Rengers, F. K., and Tucker, G. E. (2015). "Aspect-dependent soil saturation and insight into debris-flow initiation during extreme rainfall in the Colorado front range." *Geology*, 43(8), 659–662.

Feldman, A. D. (2000). *Hydrologic Modeling System Technical Reference Manual*. *Institute for Water Resources, Hydrologic Engineering Center*, Davis, CA.

FERC. (2001). *Engineering Guidelines for the Evaluation of Hydropower Projects*. *Assessment*.

Fleming, M., and Neary, V. (2004). "Continuous Hydrologic Modeling Study with the Hydrologic Modeling System." *Journal of Hydrologic Engineering*, 9(3), 175–183.

Follum, M. L., Tavakoly, A. A., Niemann, J. D., and Snow, A. D. (2017). "AutoRAPID: A Model for Prompt Streamflow Estimation and Flood Inundation Mapping over Regional to Continental Extents." *Journal of the American Water Resources Association*, 53(2), 280–299.

Gochis, D., Schumacher, R., Friedrich, K., Doesken, N., Kelsch, M., Sun, J., Ikeda, K., Lindsey, D., Wood, A., Dolan, B., Matrosov, S., Newman, A., Mahoney, K., Rutledge, S., Johnson, R., Kucera, P., Kennedy, P., Sempere-Torres, D., Steiner, M., Roberts, R., Wilson, J., Yu, W., Chandrasekar, V., Rasmussen, R., Anderson, A., and Brown, B. (2015). "The great Colorado flood of September 2013." *Bulletin of the American Meteorological Society*, 96(9), 1461–1487.

Green, W. H., and Ampt, G. A. (1911). "Studies on Soil Physics, part 1 - the flow of air and water through soils." *The Journal of Agricultural Science*, 4(1), 1–24.

Greenland, D., Burbank, J., Key, J., Klinger, L., Burbank, J., Key, J., Klinger, L., Moorhouse, J., Oaks, S., and Shankman, D. (1985). "The Bioclimates of the Colorado Front Range." *Mountain Research and Development*, 5(3), 251–262.

Horton, R. E. (1940). "An Approach Toward a Physical Interpretation of Infiltration-Capacity1." *Soil Science Society of America Journal*, 5, 399–417.

Hrachowitz, M., Bohte, R., Mul, M. L., Bogaard, T. A., Savenije, H. H. G., and Uhlenbrook, S. (2011). "On the value of combined event runoff and tracer analysis to improve understanding of catchment functioning in a data-scarce semi-arid area." *Hydrology and Earth System Sciences*, 15(6), 2007–2024.

Jarrett, R. D., and Costa, J. E. (1988). *Evaluation of the Flood Hydrology in the Colorado Front Range Using Precipitation, Streamflow, and Paleoflood Data for the Big Thompson River Basin*. Denver, CO.

Kirchner, J. W. (2006). "Getting the right answers for the right reasons: Linking measurements, analyses, and models to advance the science of hydrology." *Water Resources Research*, 42(3), 1–5.

Kirkby, M. J., and Chorley, R. J. (1967). "Throughflow, overland flow and erosion." *Hydrological Sciences Journal*, 12(3), 5–21.

Kusumastuti, D. I., Struthers, I., Sivapalan, M., and Reynolds, D. A. (2007). "Threshold effects in catchment storm response and the occurrence and magnitude of flood events: Implications for flood frequency." *Hydrology and Earth System Sciences Discussions*, 3, 3239–3277.

Leavesley, G. H., Lichty, R. W., Troutman, B. M., and Saindon, L. G. (1983). *Precipitation-Runoff Modeling System: User's Manual. Water-Resources Investigations Report 83-4238*, Denver, CO.

Li, Z. (2014). "Watershed modeling using arc hydro based on DEMs: a case study in Jackpine watershed." *Environmental Systems Research*, 3(1), 11.

Linsley, R. K. J., Kohler, M. A., and Paulhus, J. L. H. (1958). *Hydrology for Engineers. Nature*, (H. E. Davis, ed.), McGraw-Hill Book Company.

Livers, B., and Wohl, E. (2015). "An evaluation of stream characteristics in glacial versus fluvial process domains in the Colorado Front Range." *Geomorphology*, Elsevier B.V., 231, 72–82.

MacDonald, L. H., and Stednick, J. D. (2003). *Forests and Water: A State-of-the-Art Review for Colorado. CWRRI Completion Report*, Fort Collins, CO.

McCain, J. F., Hoxit, L. R., Maddox, R. A., Chappell, C. F., and Caracena, F. (1979). *Storm and Flood of July 31-August 1, 1976 in the Big Thompson River and Cache la Poudre River Basins, Larimer and Weld Counties, Colorado, Part A. Meteorology and Hydrology in Big Thompson River and Cache la Poudre River Basins. US Geological Survey Professional Paper 1115*.

McCuen, R. H. (1989). *Hydrologic Analysis and Design*. Prentice-Hall, Inc., Englewood Cliffs, NJ.

McDonnell, J. J., Sivapalan, M., Vaché, K., Dunn, S., Grant, G., Haggerty, R., Hinz, C., Hooper, R., Kirchner, J., Roderick, M. L., Selker, J., and Weiler, M. (2007). "Moving beyond heterogeneity and process complexity: A new vision for watershed hydrology." *Water Resources Research*, 43(7), 1–6.

McGuire, L. A., Rengers, F. K., Kean, J. W., Coe, J. A., Mirus, B. B., Baum, R. L., and Godt, J. W. (2016). "Elucidating the role of vegetation in the initiation of rainfall-induced shallow landslides: Insights from an extreme rainfall event in the Colorado Front Range." *Geophysical Research Letters*, 43(17), 9084–9092.

MetStat. (2018). "Storm Precipitation Analysis System (SPAS)." <https://metstat.com/storm-analysis/spas/> (Aug. 16, 2018).

Montandon, L. M., and Small, E. E. (2008). "The impact of soil reflectance on the quantification of the green vegetation fraction from NDVI." *Remote Sensing of Environment*, 112(4), 1835–1845.

Moriasi, D. N., Arnold, J. G., Van Liew, M. W., Bingner, R. L., Harmel, R. D., and Veith, T. L. (2007). "Model evaluation guidelines for systematic quantification of accuracy in watershed simulations." *American Society of Agricultural and Biological Engineers*, 50(3), 885–900.

Nash, J. E. (1957). "The form of the instantaneous unit hydrograph." *International Association of Hydrological Sciences General Assembly*, Toronto, 114–121.

Nash, J. E., and Sutcliffe, J. V. (1970). "River Flow Forecasting Through Conceptual Models Part I: A Discussion of Principles." *Journal of Hydrology*, 10, 282–290.

National Weather Service, and NOAA. (2013). *Exceedance Probability Analysis for the Colorado Flood Event 9-16 September 2013*. Silver Spring, MD.

Ogden, F. L., and Watts, B. A. (2000). "Saturated area formation on nonconvergent hillslope topography with shallow soils: A numerical investigation." *Water Resources Research*, 36(7), 1795–1804.

Pearce, A. J., Stewart, M. K., and Sklash, M. G. (1986). "Storm Runoff Generaion in Humid Headwater Catchments 1. Where Does the Water Come From." *Water Resources Research*, 22(8), 1263–1272.

Peel, M. C., Finlayson, B. L., and Mcmahon, T. A. (2007). "Updated world map of the Koppen-Geiger climate classification." *Hydrology and Earth System Sciences*, 11, 1633–1644.

Perry, M. A., Franz, J., Dick, C., and Kappel, B. (2017). "Advances in Flood Hydrology for Modeling High Elevation Mountain Basins in Colorado with Applications to the Gross Dam Enlargement Study." *Association of State Dam Safety Officials Dam Safety Conferece*, Philadelphia, Pennslyvania.

Philip, J. R. (1957). "The theory of infiltration: 1. The infiltration equation and its solution." *Soil Science*, 83, 345–357.

Rawls, A. W. J., Brakensiek, D. L., and Savabi, M. R. (1989). "Infiltration parameters for rangeland soils." *Journal of Range Management*, 42(2), 139–142.

Rawls, W. J., Brakensiek, D. L., and Miller, N. (1983). "Green-ampt Infiltration Parameters from Soils Data." *Journal of Hydraulic Engineering*, 109(1), 62–70.

Rengers, F. K., McGuire, L. A., Coe, J. A., Kean, J. W., Baum, R. L., Staley, D. M., and Godt, J. W. (2016). "The influence of vegetation on debris-flow initiation during extreme rainfall in the northern Colorado Front Range." *Geology*, 44(10), 823–826.

Sabol, G. V. (2008). *Hydrologic Basin Response Parameter Estimation Guidelines*. State of Colorado, Office of the State Engineer, Dam Safety Branch.

Saxton, K. E., and Rawls, W. J. (2006). "Soil Water Characteristic Estimates by Texture and Organic Matter for Hydrologic Solutions." *Soil Science Society of America Journal*, 70, 1569–1578.

Shanley, J. B., Sebestyen, S. D., Mcdonnell, J. J., Mcglynn, B. L., and Dunne, T. (2015). "Water's Way at Sleepers River watershed - revisiting flow generation in a post-glacial landscape, Vermont USA." *Hydrological Processes*, 29(16), 3447–3459.

Sherman, L. K. (1932). "Streamflow from rainfall by the unit hydrograph method." *Engineering News-Record*, 108, 501–505.

Sivapalan, M., Wood, E. F., and Beven, K. J. (1990). "On hydrologic similarity: 3. A dimensionless flood frequency model using a generalized geomorphologic unit hydrograph and partial area runoff generation." *Water Resources Research*, 26(1), 43–58.

Soil Survey Staff. (2019). "Soil Survey Geographic (SSURGO) Database." Natural Resources Conservation Service, United States Department of Agriculture.

Sturdevant-rees, P., Smith, J. A., Morrison, J., and Baeck, M. L. (2001). "Tropical storms and the flood hydrology of the central Appalachians." *Water Resources Research*, 37(8), 2143–2168.

Timilsina, S. (2019). "Exploring Controls on Soil Moisture and Debris Flow Initiation Patterns in the Colorado Front Range During the September 2013 Flood Event." Master of Science Thesis, Colorado State University.

Traff, D. C., Niemann, J. D., Middlekauff, S. A., and Lehman, B. M. (2015). "Effects of woody vegetation on shallow soil moisture at a semiarid montane catchment." *Ecohydrology*, 8(5), 935–947.

Troch, P. A., Smith, J. A., Wood, E. F., and de Troch, F. P. (1994). "Hydrologic controls of large floods in a small basin: central Appalachian case study." *Journal of Hydrology*, 156, 285–309.

U.S Geological Survey National Geospatial Program. (2018). "USGS National Hydrography Dataset Best Resolution for Hydrologic Unit 10." U.S. Geological Survey.

Vermote, E., Justice, C., Claverie, M., and Franch, B. (2016). "Preliminary analysis of the perforance of the Landsat 8/OLI land surface reflectance product." *Remote Sensing of Environment*, 185, 46–56.

Viessman, W. J., and Lewis, G. L. (2003). *Introduction to Hydrology*. Prentice-Hall, Inc., Upper Saddle River, NJ.

Wilkerson, J., and Merwade, V. (2010). "Incorporating Surface Storage and Slope to Estimate Clark Unit Hydrographs for Ungauged Indiana Watersheds." *Journal of Hydrologic Engineering*, 15(11), 918–930.

Xia, Y., Mitchell, K., Ek, M., Cosgrove, B., Sheffield, J., Luo, L., Alonge, C., Wei, H., Meng, J., Livneh, B., Duan, Q., and Lohmann, D. (2012). "Continental-scale water and energy flux analysis and validation for North American Land Data Assimilation System project phase 2 (NLDAS-2): 2. Validation of model-simulated streamflow." *Journal of Geophysical Research Atmospheres*, 117(D3), 1–23.

Yochum, S. E. (2015). "Colorado Front Range Flood of 2013: peak flows at flood frequencies." *3rd Joint Federal Interagency Conference on Sedimentation and Hydrologic Modeling*, Reno, Nevada, 537–548.

Zhang, Z., Koren, V., Smith, M., Reed, S., and Wang, D. (2004). "Use of Next Generation Weather Radar Data and Basin Disaggregation to Improve Continuous Hydrograph Simulations." *Journal of Hydrologic Engineering*, 9(2), 103–115.

APPENDIX A: DETAILED INSTRUCTIONS FOR DATA PRE-PROCESSING AND PARAMETER ESTIMATION

This appendix provides detailed instructions for developing the forcing data, model structure, and parameters necessary to implement the modeling methods as described in the main body of this report. The modeling methods were developed for basins in the forested and mountainous Colorado Front Range in this study. The methods incorporate principles that apply to a wide range of land covers, soil types, and geologic conditions, but their applicability to other regions needs to be assessed empirically. Caution should especially be used when applying the methods to regions where the hydrologic response may be affected by snowmelt, frozen ground, wildfire, and urban development as these factors were not considered in this study.

When applying the methods to historical storms, rainfall forcing data must be processed to adapt it to the format required for input to HEC-HMS. Significant pre-processing is required to convert rainfall data from hourly depth grids as output from SPAS to the hyetograph format that can be directly input into HEC-HMS.

The hydrologic model discussed in this study is implemented with a semi-distributed sub-basin structure. Disaggregation of the basin into sub-basins is completed to manage spatial variability of rainfall data and watershed properties. The main body of this document discusses the selection of the methods used to adequately represent the hydrologic processes occurring within each sub-basin. Section 3.2.2 Process Representation of the main document outlines the methods used for each hydrologic process. These methods can be selected in HEC-HMS under the "Subbasin" tab. Parameters must be estimated for Canopy Interception, Loss, Transform, Baseflow, and Routing processes. Section 3.3 Model Parameters outlines the parameters required for the selected methods for each process developed in this study.

Some parameters that are required within HEC-HMS for the methods used in this study are excluded in order to simplify the modeling process. Parameters could be excluded because they are unnecessary for single event simulations (i.e. Loss: GW 2 Max Storage, GW 2 Max Percolation, GW 2 Storage Coefficient) or they have minimal impact during extreme events such as those that this study focuses on (i.e. Canopy: Initial Storage; Loss: Initial GW 1 and Initial GW 2 Storage; and Baseflow: GW 1 Initial Storage).

Forcing Data
1. Rainfall:
- Instructions in this section are for historical storms in which hourly rainfall total grids were in ASCII format were developed using SPAS
    - The CO-NM Regional Extreme Precipitation Study tool should be used in developing rainfall data for design storms instead of the procedure shown here for historical storms
- Use ModelBuilder model to project ASCII rasters to UTM Zone 13N and resize to 5-10 m resolution
    - Direct path of "ASCII" bubble to folder which contains ASCII rasters
    - Direct path of %Name%_proj.tif bubble to desired location of output rasters
    - ModelBuilder model: http://www.engr.colostate.edu/~jniemann/datapage.htm
- Use Python code provided in Appendix B to calculate hourly spatial average and create hyetographs for each sub-basin: http://www.engr.colostate.edu/~jniemann/datapage.htm
    - The Python code for this process uses both Pandas and ArcPy libraries. Installing the Pandas package with the IDLE Python GUI can be difficult. For this reason, it can be simplest to split the code into two separate model runs if unfamiliar with Python. The first run uses ArcPy portion of the code and is run in IDLE; the second uses Pandas to

plot the hyetographs and can be executed in a distribution such as Enthought's Canopy. It is possible; however, to use Pandas with the IDLE GUI to run the entire code at once.
- o Required data and variables are described in the Python file
- The Python script will output hyetographs to Excel and save the file in the location that the user specifies
  - o Excel hyetographs are in incremental cm and need to be converted to mm or in for HEC-HMS input

Model Structure
2. Sub-basin Disaggregation
- Digital Elevation Model (DEM)
  - o When developing the modeling methods, DEMs for all basins were downloaded from the National Elevation Dataset (NED) to ensure consistent data quality for all hydrologic models. NED data covers the entire Front Range, and the tiles are 1/3 arc-second resolution.
  - o Re-project the DEM into the NAD83 UTM projection using the Project Raster tool
    - ▪ The entirety of the eastern plains and front range as well as much of the western slope lies within Zone 13N; only a portion of far western Colorado lies in zone 14
    - ▪ Do not change the Output Cell Size and choose Bilinear for the Resampling Technique
  - o Convert the DEM elevation values from feet to meters with the Raster Calculator tool if it is not already in meters.
- Use ArcHydro tools in ArcGIS to develop sub-basins (refer to Djokic et al. (2011) for overview)
  - o Do not use DEM reconditioning to burn stream lines into DEM prior to disaggregation
  - o Fill sinks/pits in DEM to avoid undefined flow directions
  - o Run Flow Direction tool to determine flow direction of each cell based on neighboring elevations
  - o Run Flow Accumulation tool to determine the number of cells flowing into each cell
  - o Run Stream Definition tool
    - ▪ Creates stream grid that indicates the presence/absence of a stream in each cell based on a contributing area threshold
    - ▪ Threshold of 15 km^2 was selected as consistent threshold for all basins to adequately characterize spatial variation of precipitation
  - o Run Stream Segmentation tool to separate stream grid into stream segments where confluences distinguish the ends of each segment
  - o Run Catchment Grid Delineation tool to delineate a separate sub-basin for each stream segment
  - o Run Catchment Polygon Processing tool to create sub-basin shapefiles from grid
  - o Because stream gauge location likely will not coincide with outlet of any sub-basin, use Watershed tool to delineate basin at gauge location and incorporate the basin into the sub-basin structure
- Separate sub-basins into north- and south-facing aspects
  - o Run Aspect tool with the DEM as input to calculate slope direction in degrees
  - o Run Reclassify tool on Aspect raster to specify that North includes aspects from 0°-90° and 270°-360° while South includes aspects from 90°-270° (In example below, North=2 and South=3)

Old values	New values
-1 - 0	1
0 - 90	2
90 - 270	3
270 - 360	2
NoData	NoData

- Because some cells will have no aspect (i.e. flat), use flow direction raster to assign aspect to these cells
  - Use Reclassify tool on flow direction raster to assign north-facing values to flow direction cells equal to 32, 64, and 128 and south-facing values to flow directions of 2, 4, and 8 (refer to ESRI's online help for an overview of the flow direction raster)
    - For flow direction cells exactly east or west (value=16 or 1), assign one direction to be north and the other to be south (in example below, east is assigned to be north and west is assigned to be south)
      - These can be assigned arbitrarily because they comprise a small portion of the basin and will have minimal impact on the delineation

Old values	New values
1	2
32	2
64	2
128	2
NoData	NoData
2 - 16	3

  - Assign North and South from flow direction raster to reclassified aspect raster using the Con tool

Input conditional raster
asp_reclass
Expression (optional)
"VALUE" = 1
Input true raster or constant value
fdr_reclass
Input false raster or constant value (optional)
asp_reclass
Output raster
T:\Projects\jdngroup\Doug_Research\GIS\metric\Basin_Delineations\Chey\aspect_NF_SF

- Add 'Aspect' field raster to define North and South facing cells
  - Consistent with the naming convention from the previous example, in the image below "Value=2" is assigned to be North and "Value=3" is South

	Rowid	VALUE	COUNT	ASPECT
▶	0	2	367794	North
	1	3	304079	South

  - Convert the raster to a shapefile using the Raster to Polygon tool with 'Aspect' as the new value field (do not check the simplify polygons box).
- Use NF/SF shapefile to separate the sub-basin shapefile by aspect
  - Using Dissolve tool, dissolve discontiguous features of NFS/SFS aspect shapefile into two single features (one for NFS, one for SFS)
    - Specify newly created "Aspect" field as the Dissolve Field as shown in image below

- ▪ Use Intersect tool with dissolved NFS/SFS shapefile to find north- and south-facing component of each sub-basin
  - The output of this tool is the final sub-basin shapefile with NFS and SFS components that will be used in the hydrologic model

- ▪ Create basin model in HEC-HMS with NFS and SFS sub-basins corresponding to the shapefile produced in the previous step
  - Sub-basin SFS and NFS elements will be comprised of noncontiguous areas, but they can be lumped together and treated as a single sub-basin because unit hydrograph theory assumes additivity
  - Area can be obtained from shapefile and input into HEC-HMS

Parameters

3. Canopy Interception

The instructions provided in this section assist with estimation of the *maximum canopy storage* and *potential evapotranspiration rate* parameters under the Simple Canopy. These parameters can be input into HEC-HMS under the Canopy tab.

- Based on rainfall data measured at a research catchment in the Cache la Poudre River basin (Traff et al., 2015) during September 2013 storms, the Simple Canopy model was implemented in a spreadsheet to calibrate *maximum canopy storage* and *potential evapotranspiration rate* while optimizing the NSCE in comparison with the observed throughfall data. The analysis was completed for both NFS and SFS.
- The optimized canopy capacity is 7.2 mm on NFS and 1.5 on SFS. These values can be entered as the *maximum canopy storage* under the Simple Canopy method
- The optimized depletion rate is 2.3 mm/day on NFS and 5.6 on SFS. These are applied by selecting annual evapotranspiration in the meteorological model. Enter the values in the "Rate" column.

4. Loss and Baseflow

The instructions provided in this section assist with estimation of the *initial soil storage*, *maximum infiltration rate*, *maximum soil storage*, *tension storage, maximum soil percolation rate*, *maximum GW 1 storage, maximum GW 1 percolation*, and *GW 1 storage coefficient* parameters under the Soil Moisture Accounting method and the *linear reservoir GW 1 storage coefficient* under the Linear Reservoir method. These parameters can be input into HEC-HMS under the Loss and Baseflow tabs.

The soil layer parameters were estimated primarily using the Natural Resources Conservation Service's (NRCS) Soil Survey Geographic (SSURGO) database. The soil texture data is used as an input in the Python script pedotransfer_fn.py (Appendix C) to perform a number of calculations to obtain SMA parameters. The script first uses pedotransfer functions (Saxton and Rawls, 2006; Rawls et al., 1983) to calculate the bare ground saturated hydraulic conductivity K_{sat}, porosity ϕ, field capacity θ_{fld}, wilting point θ_{wp}, and wetting front suction head ψ_f. K_{sat} is then adjusted for vegetation cover based on existing hydrology guidelines for Colorado (Sabol, 2008). The script then uses the Green-Ampt equation to calculate the maximum infiltration rate at a representative depth. Finally, the maximum and initial soil storage are calculated.

Use this portion of the document in conjunction with the Python script 'pedotransfer_fn.py' in Appendix C. Variable names below in **bold** denote files that must be created or updated by the user. The remaining variables in *italics* are created internally by the model. The user must update all file paths in the script for input, internal, and output variables. 'pedotransfer_fn.py' is used to calculate *maximum infiltration rate, maximum soil storage*, and *tension storage*. The Python script outputs these parameters as spatial average values for each sub-basin in table format.
- Sub-basin shapefile
  - Variable name in 'pedotransfer_fn.py': ***subs***
  - Sub-basin shapefile (without NFS and SFS elements) as developed previously in Section 1. Sub-basin Disaggregation
- NFS and SFS polygons
  - Variable name in 'pedotransfer_fn.py': ***aspect***
  - NFS and SFS polygons as developed previously in Section 1. Sub-basin Disaggregation
- Sub-basin shapefile with NFS and SFS elements
  - Variable name in 'pedotransfer_fn.py': ***asp_subs***
  - Sub-basin shapefile (separated into NFS and SFS elements) as developed previously in Section 1. Sub-basin Disaggregation
- Soil textures and organic matter
  - Variable names in 'pedotransfer_fn.py': ***sand***, ***clay***, and ***OM***

- o Rasters representing the percent sand, percent clay, and percent organic matter of the soil. The Python script uses the soil texture data as an input to pedotransfer functions (Saxton and Rawls, 2006; Rawls et al., 1983) to calculate the bare ground saturated hydraulic conductivity K_{sat}, porosity ϕ, field capacity θ_{fld}, wilting point θ_{wp}, and wetting front suction head ψ_f.
  - o Steps to download rasters:
    - ▪ Extract dominant percent sand, clay, and organic matter from SSURGO database
      - • Download soils data from NRCS (https://gdg.sc.egov.usda.gov/)
      - • Import map unit raster or polygon from soils data into ArcGIS
      - • Run Create Soil Map tool in Soil Data Development Toolbox for percent sand, clay, and organic matter
        - o Use Weighted Average Aggregation Method and top 45.7 cm of soil–or 18 inches per Colorado's existing guidelines for storms less frequent than the 100-yr event (Sabol, 2008)
      - • Convert shapefiles to rasters, set cell size between 5-10 m (make sure cell size is consistent for all rasters) and project to UTM Zone 13N
- • Theta parameters
  - o Variable names in 'pedotransfer_fn.py': *theta_33t*, *theta_33*, *theta_s_33t*, *theta_s_33*, *theta_s*
  - o This series of calculations is done to determine the *theta_s* parameter (porosity) using Equations 2-3 and 5 from Saxton and Rawls (2006). Additionally, *theta_33* represents the field capacity soil moisture
- • Bare ground hydraulic conductivity
  - o Variable names in 'pedotransfer_fn.py': *B*, *theta_1500t*, *theta_1500*, *lamda*, *Ksatbare*
  - o This series of calculations uses Equations 1, 15, 16, and 18 from Saxton and Rawls (2006) to calculate the bare ground hydraulic conductivity (*Ksatbare*). Additionally, *theta_1500* represents the wilting point soil moisture
- • Wetting front suction head
  - o Variable names in 'pedotransfer_fn.py': *A*, *psiet*, *psie*, *psie_head*, *psif*
  - o This series of calculations uses Equations 4 and 14 from Saxton and Rawls (2006) and Equation 4 from Rawls et. al (1983) to calculate wetting front suction head (*psif*)
- • Vegetation cover (or fractional vegetation)
  - o Variable name in 'pedotransfer_fn.py': **Vc**
  - o Fractional vegetation cover is used to adjust the bare ground K_{sat} for vegetation cover based on existing hydrology guidelines for Colorado (Sabol, 2008)
  - o Request NDVI data for area of interest from Earth Science Processing Architecture (ESPA) (https://espa.cr.usgs.gov/)
    - ▪ NDVI data has scale factor of 0.0001; use Raster Calculator to convert to unscaled NDVI
  - o Use Raster Calculator to calculate fractional vegetation per Montandon and Small (2007):

$$F_g = \left(\frac{NDVI_{pixel} - NDVI_0}{NDVI_\infty - NDVI_0}\right)^2$$

    - ▪ $NDVI_{pixel}$ is the raster that was obtained from ESPA; $NDVI_0$ is the bare soil NDVI which can be obtained by determining value of the ESPA NDVI raster in bare soil locations; $NDVI_\infty$ is the live vegetation NDVI which can be obtained by determining value of the ESPA NDVI raster in densely forested locations
- • Saturated hydraulic conductivity (adjusted for vegetation)
  - o Variable names in 'pedotransfer_fn.py': *ck*, *Ksathalf*, *Ksat*

- o The equation from Figure 6.8 of Sabol (2008) is used to adjust the saturated hydraulic conductivity based on vegetation cover. Per Bouwer (1964), hydraulic conductivity should be adjusted to ½ of the saturated hydraulic conductivity value to account for flow in the unsaturated zone.
- Maximum infiltration
  - o Variable name ins 'pedotransfer_fn.py': *delta, f, f_halfks*
  - o Green-Ampt equation is used to calculate the maximum infiltration rate (*f*) at a representative depth, δ (*delta*)
  - o δ assumed to be 3 inches

$$f = K_{sat}\left[1 + \frac{|\psi_f|}{\delta}\right]$$

$$K_{sat}: saturated\ hydraulic\ conductivity\ (Ksathalf)$$
$$\psi_f: wetting\ front\ suction\ head\ (psi\_f)$$
$$\phi: porosity\ (theta\_s)$$

  - o The full saturated hydraulic conductivity (*Ksat*) and half saturated hydraulic conductivity (*Ksathalf*) were both used in the equation to compare results, and it was determined that using *Ksathalf* produces more realistic results.
  - o *f* corresponds to *maximum infiltration rate* and can be input in the HEC-HMS model under the Loss tab
- Depth to restrictive layer
  - o Variable name in 'pedotransfer_fn.py': **d_restr**
  - o Raster of soil depth to a restrictive layer
  - o Steps to develop raster:
    - ▪ Use Soil Data Viewer to extract depth to restrictive layer
      - • Due to an error in NRCS's aggregation method with GSSURGO data, Soil Data Development Toolbox should not currently be used for depth to restrictive layer
    - ▪ Download soils data from Web Soil Survey
    - ▪ Add soil layer shapefile which defines soil polygon boundaries into ArcMap (shapefile name usually starts with soilmu_a)
    - ▪ Import tabular data into database
      - • Open .mdb database file that was downloaded from Web Soil Survey
      - • Follow "SSURGO Import" instructions that prompt user to enter path of tabular data folder
    - ▪ Run Soil Data Viewer by clicking on its icon on the toolbar
      - • Select soil layer that was previously added to map
      - • Select database that contains tabular soil data (this is the .mdb file downloaded from Web Soil Survey)
      - • Select the Depth to Any Soil Restrictive Layer tool in Soil Data Viewer and select the "Map" option
        - o Convert output shapefile to raster, set cell size consistent with soil textures and organic matter rasters, and project to UTM Zone 13N
- Maximum Soil Storage and Wilting Point Storage
  - o Variable names in 'pedotransfer_fn.py': *S_max, Si_fld, Si_wp*
  - o Maximum soil storage (*S_max*), field capacity soil storage (*Si_fld*), and wilting point soil storage (*Si_wp*) are calculated by multiplying soil depth by the corresponding soil moisture content.
  - o *S_max* corresponds to *maximum soil storage* and *Si_wp* corresponds to *tension storage*, and both parameters are input into HEC-HMS under the Loss tab

The remaining parameters are not calculated using the pedotransfer_fn.py file. The procedures used to estimate *initial soil storage*, *maximum soil percolation rate, maximum GW 1 storage, maximum GW 1 percolation*, *GW 1 storage coefficient* and *linear reservoir GW 1 storage coefficient* are described below.

- *Initial soil storage*
    - o Download NLDAS soil moisture data for immediately prior to storm (https://disc.gsfc.nasa.gov/datasets/NLDAS_MOS0125_H_V002/summary?keywords=NLDAS)
        - ▪ Select Subset / Get Data option and enter date and location
            - • File Format: NetCDF
            - • Variables: SOILM = Soil moisture content (kg/m^2)
                - o Note: units convert to 1 mm of water ($\frac{kg}{m^2} x \frac{1000\ cm^3}{m^2} x \frac{1\ m^3}{10^6\ cm^3} = 1\ mm$)
        - ▪ Import soil moisture NetCDF data into ArcGIS
            - • Use "Make NetCDF Raster Layer" tool in ArcGIS to import soil moisture data
            - • Export resulting layer to a raster that covers basin area
        - ▪ Calculate spatial average of soil moisture data by sub-basin (separated by aspect) using the Zonal Statistics as Table tool:

            - • Output is the soil moisture volume in mm
        - ▪ *Initial soil storage* can be calculated by dividing the soil moisture volume in mm by *maximum soil storage* for each sub-basin
- *Maximum GW 1 storage, maximum GW 1 percolation*, *GW 1 storage coefficient* and *linear reservoir GW 1 storage coefficient*
    - o Process for estimating subsurface flow parameters is described in detail in Fleming and Neary (2004) and Linsley et al. (1958).
    - o Plot daily average flow versus time for large storm on semi-log graph
    - o Take the natural log of linear reservoir equation and fit it to the recession of the hydrograph; this line represents the baseflow

$$Q(t) = Q_0 e^{-t/k} \rightarrow lnQ(t) = -\frac{t}{k} + lnQ_0$$

    - o Subtract the baseflow from the total storm hydrograph; the resulting hydrograph represents the interflow + surface flow
    - o SMA requires the use of a "Baseflow" linear reservoir to route interflow to the basin outlet in addition to the SMA Groundwater 1 reservoir; therefore, interflow is modeled using two linear reservoirs.
        - ▪ Take the natural log of equation for 2 linear reservoirs in series and fit to the recession of the interflow + surface flow hydrograph; this line represents interflow

56

$$Q(t) = Q_0 \frac{e^{-t/k}}{k} t \rightarrow lnQ(t) = -\frac{t}{k} + lnt + lnQ_0 - lnk$$

- This equation is used to estimate the SMA groundwater and baseflow parameters
- *GW 1 storage coefficient* and *linear reservoir GW 1 storage coefficient* = k
- *Maximum GW 1 storage* = Q_0k/A
  - o *Maximum GW 1 percolation* initially estimated to be between 1-3 mm/hr then calibrated
- *Maximum soil percolation rate* was estimated based on infiltrometer tests of weathered bedrock data in the Front Range (Ebel, 2016)
  - o The average hydraulic conductivity of the infiltrometer tests is 82.9 mm/hr
    - *Maximum soil percolation rate* = 82.9 mm/hr; input under Loss tab in HEC-HMS for all basins
5. Clark Unit Hydrograph:

Use this portion of the document in conjunction with the Python script 'Tc_model.py' in Appendix D. Variable names in **bold** denote files that must be created or updated by the user. The remaining variables are created internally by the model. The user must update all file paths in the script for input, internal, and output variables.

The instructions provided in this section assist with estimation of the Time Area Curve which describes the distribution of travel times through the sub-basin. The *time of concentration T_c* and *storage coefficient R* parameters can then be calculated from the Time Area Curve. These parameters can be input into HEC-HMS under the Transform method tab.

Time Area Curve:
- Manning's roughness:
  - o Variable name in 'Tc_model.py': ***mannings_n***
  - o Download NLCD 2011 Land Cover data from USGS National Map download (https://apps.nationalmap.gov/download/)
  - o Add Manning's n field to Land Cover raster and populate field using values in Table 6.1 from Follum et al. (2016). These values can be adjusted within the Low to High range later to ensure realistic implied channel velocities (see *chantime* variable below)
  - o Use Lookup tool and set the Lookup field as the new manning's n field that was just created
    - Input raster: land cover raster from NLCD
    - Lookup field: field which contains manning's n values
- DEM:
  - o Variable name in 'Tc_model.py': ***DEM***
  - o See Section 1. Digital Elevation Model above
  - o The elevations should be in metric
- Stream extent:
  - o Variable name in 'Tc_model.py': ***stream_extent***
  - o This variable defines the locations where the model uses channel flow equations rather than overland flow equations. The raster is created using the ArcHydro tools and varying the contributing area threshold until the extent of the streams reasonably matches what can be observed from aerial imagery. The threshold used to create this raster will be significantly smaller than the threshold in developing the sub-basins. ArcHydro tools and the contributing area threshold are explained in Section 2. Subbasin Disaggregation.
- NF and SF polygons:
  - o Variable name in 'Tc_model.py': ***asp_reclass***
  - o This shapefile contains north- and south-facing polygons and was developed by reclassifying the aspect raster. It was previously developed for Section 2. Subbasin Disaggregation.

- Flow Accumulation Raster:
  - Variable name in 'Tc_model.py': ***fac***
  - Flow accumulation raster as developed previously in Section 2. Subbasin Disaggregation.
- Flow Direction Raster:
  - Variable name in 'Tc_model.py': ***fdr***
  - Flow direction raster as developed previously in Section 2. Subbasin Disaggregation.
- Cell size
  - Variable name in 'Tc_model.py': ***cellsize***
  - A constant which represents the DEM cell size. Update this value to correspond to DEM's resolution.
- Sub-basin shapefiles:
  - Variable name in 'Tc_model.py': ***sub***
  - The *sub* variable includes separate shapefiles for each sub-basin in the watershed. A for loop is used to iterate through each sub-basin and read the appropriate sub-basin's boundary to the variable. The shapefile is used to set the extent of the analysis. The Accum_Time function that is called in Tc_model.py iterates through each cell within the shapefile's extent, so it is important to minimize the extent to increase the function's efficiency.
  - These shapefiles can be developed simply by exporting the individual features in the sub-basin shapefile created in Section 2. Sub-basin Disaggregation. Be sure to name the shapefiles consistent with the Tc_model.py script (e.g. extent_1.shp for sub-basin 1)
- DEM clipped to each sub-basin
  - Variable name in 'Tc_model.py': *DEM_sub*
  - Similar to the *sub* variable, the portion of the DEM within each sub-basin is extracted with each for loop. Each sub-basin's DEM is extracted using the Extract by Mask tool in ArcPy. The resulting DEM is the initial input to the processes within each for loop.
- Slope
  - Variable name in 'Tc_model.py': *slope*
  - The slope of each sub-basin is calculated using the ArcPy Slope tool. The resulting slope grid is in percent slope.
- Slope grid with reservoir slopes filtered out
  - Variable name in 'Tc_model.py': ***slpprcnt***
  - Low or zero slope values within reservoirs/lakes produce unrealistically low velocity values, causing portions of the sub-basins to drain too slowly. A slope threshold should be established such that slopes below the threshold are located primarily within reservoirs with minimal occurrences outside of the reservoirs. Slopes below the threshold are replaced using the ArcPy Con tool so that the new values provide a reasonable minimum flow velocity. The threshold can also be adjusted to obtain a reasonable average flow velocity for each sub-basin
  - The Con tool is already incorporated into the Python code, but the user must adjust the value to obtain reasonable minimum and average velocities. The threshold is currently set at 0.4
- Decimal slope grid
  - Variable name in 'Tc_model.py': *slpdec*
  - Converts the percent slope grid to decimal slope using the ArcPy Divide tool
- Channel slope grid
  - Variable name in 'Tc_model.py': *chanslp*
  - Extracts the channel slope from the decimal slope grid using the Extract by Mask tool and *stream_extent* as the mask.
- Flow time per channel cell grid

- o Variable name in 'Tc_model.py': *chantime*
- o The flow time per channel cell is calculated using a series of ArcPy processes. The processes include several intermediate variables that must be calculated to complete the travel time calculation. Manning's equation is used to calculate the travel time per cell:

$$t = \frac{d \cdot n}{Rh^{2/3} \cdot \sqrt{s}}$$

- o t: time per cell, d: distance (cell size), n: manning's roughness coefficient, Rh: hydraulic radius, s: slope
- o *Intermediate variables:* The hydraulic radius raster, Rh, is calculated using downstream hydraulic geometric relationships. Livers and Wohl (2014) collected bankfull depth and width measurements at 111 sites throughout the Colorado Front Range. The data were used to establish relationships for depth vs drainage area ($d = c2 \cdot DA^f$) and width vs. drainage area ($w = c1 \cdot DA^b$). The relationships are used to calculate depth and width for the entire sub-basin where DA is determined from the flow accumulation raster. The wetted perimeter, P, and flow area, A, can then be calculated. A and P are then used to calculate Rh.

- Flow velocity per overland cell grid
  - o Variable name in 'Tc_model.py': *Vel*
  - o The overland flow velocity is calculated using an approximation of manning's equation:

$$V = k \cdot \sqrt{s}$$

  - o k: roughness k-factor, s: slope
  - o 'Tc_model.py' includes two options: (1) cell-specific k-factor based on the landcover dataset, and (2) a constant k-factor that can be adjusted to achieve realistic overland velocities. Because the overland flow velocity equation is based on manning's equation, k represents the variables n and Rh. Because we have no method to estimate or measure Rh for every overland cell in the sub-basin, using a cell-specific k value implies that we know more information than we actually do. For this reason, we used the constant k-factor method for this study. Therefore, we initially set a constant k of 0.4 and adjust the value to achieve a realistic average mean velocity.

- Flow time per overland cell grid
  - o Variable name in 'Tc_model.py': *overlandtime*
  - o The overland travel time per cell is calculated as:

$$t = \frac{d}{v}$$

  - o t: travel time per overland cell, d: cell size, v: velocity grid (*Vel*)

- Combined travel time per cell raster
  - o Variable name in 'Tc_model.py': *traveltime*
  - o Uses the ArcPy tool Mosaic to New Raster to combine the overland and channel travel time rasters to create a travel time per cell raster for the entire basin.

- Accumulated travel time raster
  - o Variable name in 'Tc_model.py': *totaltime*
  - o Calls the user-defined function Accum_Time to calculate the accumulated travel time to each point in the sub-basin.
  - o Intermediate variable within Accum_Time that user must provide:
    - ▪ Variable name in 'Tc_model.py': **outs_layer**
      - Shapefile of sub-basin outlet points, which must have a field named "Id" with a value of 0. The points must be located on the cell corresponding to the highest flow accumulation within each sub-basin. If the points are placed improperly, the code could get caught in an infinite loop.
  - o The Accum_Time function calculates the accumulated travel time raster as follows:

- Extracts *traveltime* raster to sub-basin boundary and convert raster to an array for processing
- Clips flow direction raster to sub-basin boundary using Extract by Mask tool
- Replaces the outlet cell value of the flow direction raster of each sub-basin with a value of zero using the Point to Raster and Mosaic to New Raster tools. This step is completed because the algorithm used by this function iterates through the sub-basin until it reaches a flow direction value of zero. The new flow direction raster is named *fdrout*.
- Creates array of *fdrout* for processing using the Raster to NumPy Array tool
- Creates empty array with the same dimensions as the flow direction array
- Iterates through the time array and change any negative values to zero
- Iterates through each cell in the sub-basin's array and calculates the travel time to the outlet for each cell. The code first checks to ensure the current cell is located within the sub-basin. If it is, the code then follows the flow direction raster to the basin's outlet, accumulating the individual cell travel times along the way. Once it reaches the basin outlet, the total accumulated travel time is assigned to that cell.
- Converts the accumulated travel time array to a georeferenced raster so that it can be viewed in ArcMap.
- Cumulative Density Function of travel times (CDF for entire sub-basin is calculated first, then separate CDFs for NFS and SFS are completed in a for loop)
  - Variable name in 'Tc_model.py': *Perc_Time* and *Perc_Area*
  - *Perc_Area* and *Perc_Time* are plotted as the x and y ordinates, respectively, of the cumulative distribution function. This plot is used as an input to HEC-HMS as the Time-Area Method Percentage Curve under the Transform tab.

Time of Concentration and Storage Coefficient:
- Since the *time of concentration T_c* is the time of travel of the hydraulically most distant point in a basin, it is determined to be equal to the longest time from the time-area curve. The *storage coefficient R* is then calculated using methods developed by Sabol (2008):

$$R = 0.37 T_c^{1.11} L^{0.8} A^{-0.57}$$

  - R: storage coefficient (hr), Tc: time of concentration (hr), L: length of watercourse to hydraulically most distant point (miles), A: area (mi^2)
  - These values can be input into HEC-HMS under the Transform tab

6. Routing

The instructions provided in this section assist with estimation of the *Length (m)*, *Slope (m/m)*, *Manning's n, Cross Section, Left Manning's n,* and *Right Manning's n* parameters under the Muskingum-Cunge with Eight Point Cross Section method. These parameters can be input into HEC-HMS under the Routing tab.
- *Length (m)*, *Slope (m/m),* and *Cross Section*
  - *Length (m)* and *Slope (m/m)* are measured from aerial imagery and the DEM
  - *Cross Section*
    - Assume rectangular channel
    - Channel width data is obtained from aerial imagery and the DEM
    - Flow depth is calculated iteratively using Manning's equation and assuming a flow that is half of the maximum flow during the storm of interest
    - Floodplain width is measured from the DEM
- *Manning's n, Left Manning's n,* and *Right Manning's n*

o Estimated based on channel type and floodplain vegetation based on aerial imagery and representative roughness values (Chow, 1959)

APPENDIX B: PYTHON CODE FOR HYETOGRAPH DEVELOPMENT

```
###
#
# Description: The following code is used to convert hourly rainfall depth grids for a storm to
# hyetograph format that can be input in HEC-HMS.
#
###
from dbfread import DBF
import pandas as pd
from pandas import DataFrame
import numpy as np
import datetime
import matplotlib.pyplot as plt
from  matplotlib.dates import DayLocator
import arcpy
arcpy.CheckOutExtension("Spatial")
arcpy.env.overwriteOutput = True

Chey_Subs = "T:\\projects\\jdngroup\\XXXX\\20180925_Chey_Subs.shp" # shapefile of sub-basin
network for basin
asp_reclass = "T:\\projects\\jdngroup\\XXXX\\chey_nf_sf.shp" # shapefile of NF and SF slopes
asp_subs = "T:\\projects\\jdngroup\\XXXX\\20180925_Chey_Subs_asp.shp" # shapefile of sub-basins
separated into NF and SF slopes

d_North=np.empty([1,3]) # change based on number of sub-basins
d_South=np.empty([1,3]) # change based on number of sub-basins
h=0 #initialize counter
t=datetime.datetime(2013,9,8,8)  #initialize time counter, set as first hour of storm
tarray=np.empty([1,1])
xlabels=np.empty([1,1])
aspect=['NFS','SFS']

# use for loop to iterate through each hour of storm
for x in range(0,240):# change the upper limit in the range to equal the duration of the storm in hours
    hr=str(t.hour).zfill(2)+"00" #extract current hour
    day=str(t.day).zfill(2) #extract current day
    print(x)
    # use for loop to iterate through NFS and SFS
    for y in aspect:
        # Define precipitation grid for each hour

precip=("T:\projects\jdngroup\XXXX\P_allsites_spas1302_"+str(h+1).zfill(3)+"_201309"+day+"_"+hr+"
_utc_ascii.asc_proj.tif")  # change path to location of rainfall depth grids

        ## Calculate spatial average precip for each aspect for each hour in .dbf table format
        if y == 'NFS':
            table_North=("T:\projects\jdngroup\XXXX\mean_201309"+day+hr+"North"+".dbf") # change
path to desired location for table to be output
            arcpy.MakeFeatureLayer_management(asp_subs,"asp_layer")
```

```python
        arcpy.SelectLayerByAttribute_management ("asp_layer", "NEW_SELECTION",
"""{0}='{1}'""".format("ASPECT",'North'))
        tempEnvironment0 = arcpy.env.extent
        arcpy.env.extent = Chey_Subs
        arcpy.gp.ZonalStatisticsAsTable_sa("asp_layer","Name", precip,table_North,"DATA", "MEAN")
        arcpy.env.extent = tempEnvironment0

        ## Convert hourly tables into total storm hyetograph for each sub-basin
        dbf_North=DBF(table_North)
        print(dbf_North)
        df_North=DataFrame(iter(dbf_North), columns=['NAME','COUNT','AREA','MEAN'])
        print (df_North)
        s_North=np.array(df_North['MEAN'])
        d_North=np.vstack([d_North,s_North])
     else:
        table_South=("T:\projects\jdngroup\XXXX\mean_201309"+day+hr+"South"+".dbf") # change
path to desired location for table to be output
        tempEnvironment0 = arcpy.env.extent
        arcpy.env.extent = Chey_Subs
        arcpy.MakeFeatureLayer_management(asp_subs,"asp_layer")
        arcpy.SelectLayerByAttribute_management ("asp_layer", "NEW_SELECTION",
"""{0}='{1}'""".format("ASPECT",'South'))
        arcpy.gp.ZonalStatisticsAsTable_sa("asp_layer","Name", precip,table_South,"DATA", "MEAN")
        arcpy.env.extent = tempEnvironment0

        ## Convert hourly tables into total storm hyetograph for each sub-basin
        dbf_South=DBF(table_South)
        df_South=DataFrame(iter(dbf_South), columns=['NAME','COUNT','AREA','MEAN'])
        s_South=np.array(df_South['MEAN'])
        d_South=np.vstack([d_South,s_South])
    tarray=np.append(tarray,str(t.month)+"/"+str(t.day)+" "+str(t.hour)+":00")
    t=t+datetime.timedelta(hours=1)
    h+=1
    print (t)

## fill pandas with storm hyetograph arrays
d_North=np.delete(d_North,0,0)
d_South=np.delete(d_South,0,0)
d_North=np.multiply(2.54,d_North) # convert precip from inches to cm
d_South=np.multiply(2.54,d_South)
tarray=np.delete(tarray,0,0)
clmns=['Subbasin 1','Subbasin 2','Subbasin 3']
hyeto_North=pd.DataFrame(d_North,index=tarray,columns=clmns)
hyeto_South=pd.DataFrame(d_South,index=tarray,columns=clmns)

## save hyetographs to Excel
writer = pd.ExcelWriter(r"T:\projects\jdngroup\XXXX\aspect_subs_hyetograph.xlsx") # change path to
desired location for excel hyetographs to be output
hyeto_North.to_excel(writer, sheet_name='North')
hyeto_South.to_excel(writer, sheet_name='South')
writer.save()
```

```python
hyeto = [hyeto_North, hyeto_South]
## plot hyetographs
for y in range(0,3):
    s=0
    for x in hyeto:


        ycum = x[str(clmns[y])].cumsum()
        ax1=x.plot(use_index=True,y=clmns[y], secondary_y=['ycum'],kind='bar', legend=None,
stacked=True)
        ax2=ycum.plot(use_index=True, secondary_y=True, label='Cumulative Precip (cm)', linestyle='--
',linewidth=.5, color='r')
        ax1.set_xticklabels(x.index,rotation=60)
        n = 24
        ticks = ax1.xaxis.get_ticklocs()
        ticklabels = [l.get_text() for l in ax1.xaxis.get_ticklabels()]
        ax1.xaxis.set_ticks(ticks[::n])
        ax1.xaxis.set_ticklabels(ticklabels[::n])

        ax1.set_ylabel('Precipitation (cm/hr)', fontsize=12)
        ax2.set_ylabel('Cumulative Precipitation (cm)', fontsize=12)

        plt.title(str(clmns[y])+' '+str(aspect[s])+' Hyetograph', fontsize=15)
        plt.tight_layout()
        plt.savefig("T:\projects\jdngroup\XXXX\Hyeto_"+str(clmns[y])+' '+str(aspect[s])+".jpg") # change
path to desired location for hyetograph image
        plt.close('all')
        s+=1
```

APPENDIX C: PYTHON CODE FOR DEVELOPING SMA PARAMETERS

```
###
# This code is used to calculate the hydraulic properties of soils in a model based on
# percent sand, percent clay, percent organic matter, and depth to restricting layer.
# The soil properties are input into Pedotransfer functions (Saxton and Rawls, 2006; Rawls et al, 1983)
# to calculate the hydraulic properties.  Refer to Appendix A of Woolridge (2019)
# for detailed instructions on creating input files and executing the code.
#
# Created by: Douglas Woolridge
# Colorado State University
#
###

import numpy as np
import arcpy
import math
from arcpy.sa import *
from arcpy.conversion import *
arcpy.CheckOutExtension("Spatial")
arcpy.CheckOutExtension("3D")
arcpy.env.overwriteOutput = True

sand = "T:\\Projects\\jdngroup\\XXXX\\psand_0_18in" # % sand raster from SSURGO
clay = "T:\\Projects\\jdngroup\\XXXX\\pclay_0_18in" # % clay raster from SSURGO
OM = "T:\\Projects\\jdngroup\\XXXX\\OM_0_18in" # % organic matter raster from SSURGO
subs = "T:\\projects\\jdngroup\\XXXX\\20180925_Chey_Subs.shp" # sub-basin shapefile
aspect = "T:\\Projects\\jdngroup\\XXXX\\chey_nf_sf_polys.shp" # shapefile of nfs and sfs polygons
d_restr = "T:\\projects\\jdngroup\\XXXX\\d_restrwa_sdv" #depth to restricting layer raster from
SSURGO
Vc = Raster("T:\\projects\\jdngroup\\XXXX\\fg_epas") # vegetation cover raster from NDVI
asp_subs = "T:\\Projects\\jdngroup\\XXXX\\20180925_Chey_Subs_asp.shp" # shapefile of sub-basins
separated into NF and SF slopes


def Pedotransferfn(sand,aspect,clay,OM,sub,d_restr,Vc,asp_subs):

    ## set extent of sand, silt, clay, OM Rasters

    tempEnvironment0 = arcpy.env.extent
    tempEnvironment1 = arcpy.env.cellSize
    tempEnvironment2 = arcpy.env.snapRaster
    arcpy.env.extent = sub
    arcpy.env.cellSize = sub
    arcpy.env.snapRaster = sub
    sandsub = ExtractByMask(sand,sub)
    claysub = ExtractByMask(clay,sub)
    OMsub = ExtractByMask(OM,sub)

    # Convert % to fraction
```

```
sandsub = sandsub / 100
claysub = claysub / 100
OMsub = OMsub / 100


## calculate theta_s with pedotransfer functions from Saxton and Rawls (2006); Eqs 2-3, 5
theta_33t = -0.251*sandsub + 0.195*claysub + 0.011*OMsub + 0.006*sandsub*OMsub -
0.027*claysub*OMsub + 0.452*sandsub*claysub + 0.299
theta_33 = theta_33t + 1.283*theta_33t**2 - 0.374*theta_33t - 0.015 # field capacity soil moisture
theta_s_33t = 0.278*sandsub + 0.034*claysub + 0.022*OMsub - 0.018*sandsub*OMsub -
0.027*claysub*OMsub - 0.584*sandsub*claysub + 0.078
theta_s_33 = theta_s_33t + (0.636*theta_s_33t - 0.107)
theta_s = "T:\\Projects\\jdngroup\\XXXX\\theta_s" # change path to desire location of output
if arcpy.Exists(theta_s):
    arcpy.Delete_management(theta_s)
theta_s = theta_33 + theta_s_33 - 0.097*sandsub + 0.043
theta_s.save("T:\\Projects\\jdngroup\\XXXX\\theta_s") # change path to desire location of output
theta_33.save("T:\\Projects\\jdngroup\\XXXX\\theta_33") # change path to desire location of output


## calculate bare ground Ksat with pedotransfer functions from Saxton and Rawls (2006); Eqs 15, 1,
18, 16
B = "T:\\Projects\\jdngroup\\XXXX\\B" # change path to desire location of output
theta_1500t = -0.024*sandsub + 0.487*claysub + 0.006*OMsub + 0.005*sandsub*OMsub -
0.013*claysub*OMsub + 0.068*sandsub*claysub + 0.031
theta_1500 = theta_1500t + (0.14*theta_1500t-0.02) # wilting point soil moisture
theta_1500.save("T:\\Projects\\jdngroup\\XXXX\\theta_1500") # change path to desire location of
output
B = 3.817/(Ln(theta_33) - Ln(theta_1500))
lamda = 1/B
Ksatbare = "T:\\Projects\\jdngroup\\XXXX\\Ksatbare" # change path to desire location of output
if arcpy.Exists(Ksatbare):
    arcpy.Delete_management(Ksatbare)
Ksatbare = 1930*(theta_s - theta_33)**(3 - lamda)
Ksatbare.save("T:\\Projects\\jdngroup\\XXXX\\Ksatbare") # change path to desire location of output
B.save("T:\\Projects\\jdngroup\\XXXX\\B") # change path to desire location of output
lamda.save("T:\\Projects\\jdngroup\\XXXX\\lamda") # change path to desire location of output


## calculate psi_f using Saxton and Rawls, 2006 (Eqs 14, 4) and Rawls et al, 1983 (Eq. 4)
A = Exp(3.497 + B*Ln(theta_33))
psif = "T:\\Projects\\jdngroup\\XXXX\\psif" # change path to desire location of output
if arcpy.Exists(psif):
    arcpy.Delete_management(psif)
psiet = -21.67*sandsub - 27.93*claysub - 81.97*theta_s_33 + 71.12*(sandsub*theta_s_33) +
8.29*claysub*theta_s_33 + 14.05*sandsub*claysub + 27.16
psie = psiet + (0.02*psiet**2-0.113*psiet-0.7) # bubbling pressure in kPa from Saxton and Rawls,
2006
psie_head = psie / 9.81 * 1000 # kPa = 1000 N/m2 = 1000 (kg*m/s2) / m2 => head = P / rho*g => h =
[1000 (kg * m/s2) / m2] / [(1000 kg/m3)(9.81 m/s2)]; in meters, then multiply by 1000 to convert to mm

psif = (2*lamda+3)/(2*lamda+2)*(psie_head/2) # wetting front section head in mm; Eq 4 from Rawls
et al, 1983
psif.save("T:\\Projects\\jdngroup\\XXXX\\psif") # change path to desire location of output
```

```
## adjust bare ground ksat based on vegetation using Figure 6.8 in Sabol, 2008
ck = (Vc*100-10)/90 + 1
Ksat = Ksatbare*ck
Ksathalf = Ksat/2
Ksat.save("T:\\Projects\\jdngroup\\XXXX\\Ksat") # change path to desire location of output
Ksathalf.save("T:\\Projects\\jdngroup\\XXXX\\Ksathalf") # change path to desire location of output
ck.save("T:\\Projects\\jdngroup\\XXXX\\ck") # change path to desire location of output

## calculate maximum infiltration capacity based on Green-Ampt at representative depth
delta = 76.2 # representative depth of 3 inches in mm
f = "T:\\Projects\\jdngroup\\XXXX\\maxinfil" # change path to desire location of output
if arcpy.Exists(f):
    arcpy.Delete_management(f)
f = Ksat * (1 + psif/delta)
f_halfks = Ksathalf * (1 + psif/delta)
f.save("T:\\Projects\\jdngroup\\XXXX\\maxinfil") # change path to desire location of output
f_halfks.save("T:\\Projects\\jdngroup\\XXXX\\f_halfks") # change path to desire location of output

## calculate maximum soil storage as depth * porosity * 10 (cm to mm)
S_max = d_restr * theta_s * 10
S_max.save("T:\\Projects\\jdngroup\\XXXX\\S_max") # change path to desire location of output
Si_fld = d_restr * theta_33 * 10
Si_fld.save("T:\\Projects\\jdngroup\\XXXX\\Si_fld") # change path to desire location of output
Si_wp = d_restr * theta_1500 * 10
Si_wp.save("T:\\Projects\\jdngroup\\XXXX\\Si_wp") # change path to desire location of output

## calculate statistics of all soil properties by sub-basin
arcpy.env.workspace = "T:\\Projects\\jdngroup\\XXXX\\Soil_pedotransfer" #change the workspace
path to indicate where sub-basin average tables should be saved
S_max_table = ZonalStatisticsAsTable(asp_subs,"Name",S_max,"S_max_table_WA") # 'Soil Storage
(mm)'
Si_fld_table = ZonalStatisticsAsTable(asp_subs,"Name",Si_fld,"Si_fld_table")
Si_wp_table = ZonalStatisticsAsTable(asp_subs,"Name",Si_wp,"Si_wp_table") # 'Tension Storage
(mm)'
f_table = ZonalStatisticsAsTable(asp_subs,"Name",f,"f_table")
f_halfks_table = ZonalStatisticsAsTable(asp_subs,"Name",f_halfks,"f_halfks_table") # 'Max
Infiltration (mm/hr)'
psif_table = ZonalStatisticsAsTable(asp_subs,"Name",psif,"psif_table")
Ksat_table = ZonalStatisticsAsTable(asp_subs,"Name",Ksat,"Ksat_table")
Ksathalf_table = ZonalStatisticsAsTable(asp_subs,"Name",Ksathalf,"Ksathalf_table")
Ksatbare_table = ZonalStatisticsAsTable(asp_subs,"Name",Ksatbare,"Ksatbare_table")
theta_s_table = ZonalStatisticsAsTable(asp_subs,"Name",theta_s,"theta_s_table")
theta_33_table = ZonalStatisticsAsTable(asp_subs,"Name",theta_33,"theta_fld")
theta_1500_table = ZonalStatisticsAsTable(asp_subs,"Name",theta_1500,"theta_wp")

arcpy.env.extent = tempEnvironment0
arcpy.env.cellSize = tempEnvironment1
arcpy.env.snapRaster = tempEnvironment2
return f, Ksat, theta_s, psif
f,Ksat,theta_s,psi = Pedotransferfn(sand, aspect, clay, OM,subs,d_restr,Vc,asp_subs)
```

APPENDIX D: PYTHON CODE FOR DEVELOPING CLARK UNIT HYDROGRAPH PARAMETERS

```
###
# Accum_Time_function.py
#
# Description:
# This function accumulates the travel times to the sub-basin outlet for each point in the sub-basin. Two for loops are used to iterate
# through each cell in the sub-basin. For each cell, the algorithm routes through the sub-basin based on the flow direction raster.
# Refer to Appendix A of Woolridge (2019) for additional information on using the script
#
# Created by: Doug Woolridge
# Colorado State University
#
###
import numpy as np
import arcpy
import math
from arcpy.sa import *
from arcpy.conversion import *
arcpy.CheckOutExtension("Spatial")
arcpy.CheckOutExtension("3D")
arcpy.env.overwriteOutput = True


def Accum_Time(outlet,sub,fdr,travelt,cellsize):
    ## convert time raster to array
    tempEnvironment0 = arcpy.env.extent
    arcpy.env.extent = sub
    t_cellsub = ExtractByMask(travelt,sub)
    t_cellarr=arcpy.RasterToNumPyArray(t_cellsub, nodata_to_value=0)
    arcpy.env.extent = tempEnvironment0
    print('time array complete')

    ## Pre-process fdr raster and create empty array with same size as sub-basin
    # clip fdr to watershed, replace outlet value with 0, and create array from raster
    tempEnvironment0 = arcpy.env.extent
    tempEnvironment1 = arcpy.env.cellSize
    tempEnvironment2 = arcpy.env.snapRaster
    arcpy.env.extent = sub
    arcpy.env.cellSize = sub
    arcpy.env.snapRaster = sub
    fdr_sub = ExtractByMask(fdr,sub) # extract flow direction raster for sub-basin
    outrast = "T:\\projects\\jdngroup\\XXXX\\outrast"
    arcpy.PointToRaster_conversion(outlet,"Id", outrast) # convert outlet point shapefile to a raster; the
shapefile should have an "Id" field with a value of 0 so that the raster cells have a value of 0
    arcpy.env.workspace = "T:\\projects\\jdngroup\\XXXX\\ClarkUH" # change path to the same folder
where fdr_sub and outrast are saved
```

```
    arcpy.gp.MosaicToNewRaster_management([fdr_sub, outrast],
"T:\\projects\\jdngroup\\XXXX\\ClarkUH","fdrout","T:\\projects\\jdngroup\\XXXX\\20180925_Chey_Su
bs_asp.prj","8_BIT_UNSIGNED","9.1587504","1","LAST") # merge fdr raster with outlet point raster;
this creates a flow direction raster with outlet cells of value=0
    fdrout = "T:\\projects\\jdngroup\\XXXX\\fdrout" # flow direction raster with outlet cells having a value
of 0
    fdrarr=arcpy.RasterToNumPyArray(fdrout) # create array of fdrout raster
    print('fdr array complete')

    a=np.size(fdrarr,0) #rows # create empty array with same size as watershed
    b=np.size(fdrarr,1) #columns
    Travel_matrix=np.zeros((a,b))
    arcpy.env.extent = tempEnvironment0
    arcpy.env.cellSize = tempEnvironment1
    arcpy.env.snapRaster = tempEnvironment2

    ## clean array
    for i in np.arange(0,a,1):      #The for loop is used to set any negative data to zero for the travel time
raster
        for j in np.arange(0,b,1):
            if t_cellarr[i,j] < 0 or math.isnan(t_cellarr[i,j]):
                t_cellarr[i,j] = 0
    print('raster cleaned')

    ## print check to make sure all arrays have the same dimensions
    print (a, b)
    print (np.shape(fdrarr))
    print (np.shape(t_cellarr))
    print(np.shape(Travel_matrix))
    fdrcsv = np.savetxt("T:\\projects\\jdngroup\\XXXX\\fdrarr.csv",fdrarr) # save fdr array to csv
    tcellcsv = np.savetxt("T:\\projects\\jdngroup\\XXXX\\tcellarr.csv",t_cellarr) # save travel time array to
csv

    for i in np.arange(0,a,1):              # The for loop iterates through each row and column to calculate the
travel time to the outlet for each cell
        for j in np.arange(0,b,1):
            print ('cell: ', i,j)
            #print (fdrarr[i,j])
            if fdrarr[i,j]!=255:         # the flow direction raster has a value of 255 outside the extent of the
sub-basin; the if statement checks that the current cell is in the sub-basin
                p=i                 # set p and q as index of current cell
                q=j
                Travel_matrix[i,j] = t_cellarr[p,q]         # Travel_matrix stores the travel time to the sub-basin
outlet of each cell. It is given an initial value of the travel time through itself.
                while fdrarr[p,q] != 0:              # The while loop routes through sub-basin by following the
flow direction raster and adding the travel time through each cell from the t_cellarr array to the
Travel_matrix
                    if fdrarr[p,q]==1:                  # as it passes through. When the fdrarr value of the current
cell is 0 (i.e. the outlet), the final time is stored in the to cell i,j in the Travel_matrix
                        p=p
                        q=q+1
```

```
        if fdrarr[p,q]==2:
           p=p+1
           q=q+1
        if fdrarr[p,q]==4:
           p=p+1
           q=q
        if fdrarr[p,q]==8:
           p=p+1
           q=q-1
        if fdrarr[p,q]==16:
           p=p
           q=q-1
        if fdrarr[p,q]==32:
           p=p-1
           q=q-1
        if fdrarr[p,q]==64:
           p=p-1
           q=q
        if fdrarr[p,q]==128:
           p=p-1
           q=q+1

        Travel_matrix[i,j] = Travel_matrix[i,j]+t_cellarr[p,q]


    tempEnvironment0 = arcpy.env.outputCoordinateSystem
    tempEnvironment1 = arcpy.env.snapRaster
    arcpy.env.outputCoordinateSystem = arcpy.SpatialReference(26913)
    arcpy.env.snapRaster = sub
    Accum_time = "T:\\projects\\jdngroup\\XXXX\\Accum_time"
    Accum_time =
arcpy.NumPyArrayToRaster(Travel_matrix,arcpy.Point(fdr_sub.extent.XMin,fdr_sub.extent.YMin),cellsi
ze,cellsize)
    Accum_time.save("T:\\projects\\jdngroup\\XXXX\\Accum_time")
    Accumcsv = np.savetxt("T:\\projects\\jdngroup\\XXXX\\accumarr.csv",Travel_matrix)
    arcpy.env.outputCoordinateSystem = tempEnvironment0
    arcpy.env.snapRaster = tempEnvironment1
    print ('complete')

    return Accum_time
```